Fixed-t subtracted dispersion relations for Compton scattering off the nucleon

D. Drechsel, M. Gorchtein, B. Pasquini and M. Vanderhaeghen
Institut für Kernphysik, Johannes Gutenberg Universität, D-55099 Mainz, Germany
(February 7, 2008)

Abstract

We present fixed-t subtracted dispersion relations for Compton scattering off the nucleon at energies $E_\gamma \leq 500$ MeV, as a formalism to extract the nucleon polarizabilities with a minimum of model dependence. The subtracted dispersion integrals are mainly saturated by πN intermediate states in the s-channel $\gamma N \to \pi N \to \gamma N$ and $\pi\pi$ intermediate states in the t-channel $\gamma\gamma \to \pi\pi \to N\bar{N}$. For the subprocess $\gamma\gamma \to \pi\pi$, we construct a unitarized amplitude and find a good description of the available data. We show results for Compton scattering using the subtracted dispersion relations and display the sensitivity on the scalar polarizability difference $\alpha - \beta$ and the backward spin polarizability γ_π, which enter directly as fit parameters in the present formalism.

PACS : 13.60.Fz, 11.55.Fv, 14.20.Dh, 13.40.-f

I. INTRODUCTION

Compton scattering off the nucleon is determined by 6 independent helicity amplitudes A_i (i = 1,...,6), which are functions of two variables, e.g. the Lorentz invariant variables ν (related to the *lab* energy of the incident photon) and t (related to the momentum transfer to the target). In the limit $\nu \to 0$, the general structure of these amplitudes is governed by low energy theorems (LET) based on Lorentz and gauge invariance. These theorems require that (I) the leading term in the expansion in ν is determined by the global properties of the nucleon, i.e. its charge, mass and anomalous magnetic moment, and (II) the internal structure shows up only at relative order ν^2 and can be parametrized in terms of polarizabilities. In this way there appear 6 polarizabilities for the nucleon, the familiar electric and magnetic (scalar) polarizabilities α and β respectively, and 4 spin (vector) polarizabilities γ_1 to γ_4. These polarizabilities describe the response of the system to an external quasistatic electromagnetic field, and as such they are fundamental structure constants of the composite system. In particular, these polarizabilities allow one to make contact with classical physics phenomena, the dielectric constant and the magnetic permeability of macroscopic media as well as the Faraday effect in the case of the spin polarizabilities.

As a consequence of LET, the differential cross section for $\nu \to 0$ is given by the (model

independent) Thomson term. In a low-energy expansion, the electric and magnetic polarizabilities then appear as interference between the Thomson term and the subleading terms, i.e. as contribution of $O(\nu^2)$ in the differential cross section, and α and β can in principle be separated by studying the angular distributions. However, it has never been possible to isolate this term and thus to determine the polarizabilities in a model independent way. The obvious reason is that, for sufficiently small energies, say $\nu \leq 40$ MeV, the structure effects are extremely small and hence the statistical errors for the polarizabilities large. At larger energies, however, the higher terms of the expansion, $O(\nu^4)$, become increasingly important. Therefore, a reliable theoretical estimate of these higher terms is of utmost importance. Moreover, at that order also the spin-dependent polarizabilities come into the game, which has the further consequence that a full determination of the 6 polarizabilities will require an experimental program with polarized photons and polarized nucleons.

With the advent of high duty-factor electron accelerators and laser backscattering techniques, new precision data have been obtained in the 90's and more experiments are expected in the near future. In 1991 the Illinois group [1] measured differential cross sections with tagged photons at low energy. As was to be expected, the small counting rate and the low sensitivity to structure effects allowed for a reduced statistical precision only. Shortly after, Zieger et al. [2] determined the cross section for photon scattering at $\theta = 180^\circ$ by detecting the recoil proton in a magnetic spectrometer. In a series of experiments, the Illinois-Saskatoon group then studied angular and energy distributions over a wider range. Hallin et al. [3] investigated the region from pion production threshold to the $\Delta(1232)$ resonance with a high duty-factor bremsstrahlung beam. Though the statistical and systematical errors were small, the range of energy was clearly outside of the low-energy expansion. The presently most accurate values for the proton polarizabilities were derived from the work of MacGibbon et al. [4] whose experiments were performed with tagged photons at 70 MeV$\leq \nu \leq$ 100 MeV and untagged ones at the higher energies, and analyzed in collaboration with L'vov [5] by means of dispersion relations (in the following denoted by DR) at constant t. The final results were

$$\begin{aligned} \alpha &= (12.1 \pm 0.8 \pm 0.5) \times 10^{-4}\,\mathrm{fm}^3\,, \\ \beta &= (2.1 \mp 0.8 \mp 0.5) \times 10^{-4}\,\mathrm{fm}^3\,. \end{aligned} \tag{1}$$

The physics of the $\Delta(1232)$ and higher resonances has been the objective of further recent investigations with tagged photons at Mainz [6,7] and with laser-backscattered photons at Brookhaven [8]. The measured differential cross sections and polarization asymmetries helped to discard a long-standing problem, a unitarity violation reported in earlier experiments, and provided useful cross-checks for the magnetic dipole and electric quadrupole excitation of the Δ resonance. Such data were also used to give a first prediction for the so-called backward spin polarizability of the proton, i.e. the particular combination $\gamma_\pi = \gamma_1 + \gamma_2 + 2\gamma_4$ entering the Compton spin-flip amplitude at $\theta = 180^\circ$ [8],

$$\gamma_\pi = -\left[27.1 \pm 2.2(\mathrm{stat}+\mathrm{syst})\, {}^{+2.8}_{-2.4}(\mathrm{model})\right] \times 10^{-4}\,\mathrm{fm}^4\,. \tag{2}$$

In 1991 Bernard et al. [9] evaluated the one-loop contributions to the polarizabilities in the

framework of relativistic chiral perturbation theory (ChPT), with the result $\alpha = 10 \cdot \beta = 12.1$, (here and in the following, the scalar polarizabilities are given in units of 10^{-4} fm^3). In order to have a systematic chiral power counting, the calculation was then repeated in heavy baryon ChPT [10] to $O(p^3)$, the expansion parameter being an external momentum or the quark mass. The result explained the small value of the magnetic polarizability, which had been difficult to obtain in quark model calculations. A further calculation to $O(p^4)$ resulted in the values $\alpha = 10.5 \pm 2.0$ and $\beta = 3.5 \pm 3.6$, the errors being due to 4 counter terms entering to that order, which were estimated by resonance saturation [11]. One of these counter terms describes the paramagnetic contribution of the $\Delta(1232)$, which is partly cancelled by large diamagnetic contributions of pion-nucleon loops.

In view of the importance of the Δ resonance, Hemmert, Holstein and Kambor [12] proposed to include the Δ as a dynamical degree of freedom. This added a further expansion parameter, the difference of the Δ and nucleon masses ("ϵ expansion"). A calculation to $O(\epsilon^3)$ yielded the results [13] (see also Ref. [14])

$$\begin{aligned} \alpha &= 12.2 + 0 + 4.2 = 16.4 \ , \\ \beta &= 1.2 + 7.2 + 0.7 = 9.1 \ , \end{aligned} \tag{3}$$

where the 3 terms on the rhs are the contributions of pion-nucleon loops (identical to the predictions of the $O(p^3)$ calculation), Δ pole terms, and pion-Δ loops. These predictions are clearly at variance with the data, in particular $\alpha + \beta = 25.5$ is nearly twice the rather precise value determined from DR (see below). In an optimistic view the problem is to be cured by an $O(\epsilon^4)$ calculation, which is likely to produce a large diamagnetism as observed by Ref. [11]. On the other hand, a pessimist might doubt that the expansion converges sufficiently well before the higher orders have introduced a host of unknown counter terms.

The spin polarizabilities have been calculated in both relativistic one-loop ChPT [10,15] and heavy baryon ChPT [14]. In the latter approach the predictions are

$$\begin{aligned} \gamma_0 &= 4.6 - 2.4 - 0.2 + 0 = +2.0 \ , \\ \gamma_\pi &= 4.6 + 2.4 - 0.2 - 43.5 = -36.7 \ , \end{aligned} \tag{4}$$

where the spin polarizabilities are given here and in all of the following in units of 10^{-4} fm^4. The 4 separate contributions on the rhs of Eq. (4) refer to Nπ-loops, Δ-poles, $\Delta\pi$-loops, and the triangle anomaly, in that order. It is obvious that the anomaly or π^0-pole contribution is by far the most important one, and that it would require surprisingly large higher order contributions $O(\epsilon^4)$ to increase γ_π to the value of Ref. [8]. Similar conclusions were reached in the framework of DR. Using the framework of DR at $t = $ const of Ref. [5], Ref. [16] obtained a value of $\gamma_\pi = -34.3$, while L'vov and Nathan [17] worked in the framework of backward DR and predicted $\gamma_\pi = -39.5 \pm 2.4$. In the latter approach the dispersion integral is drawn along a line $t(\nu)$ corresponding to backward Compton scattering, i.e. on the lower boundary of the physical s-channel region, which is then complemented by a path into the physical t-channel region.

As we have stated before, the most quantitative analysis of the experimental data has been provided by dispersion relations. In this way it has been possible to reconstruct the forward non spin-flip amplitude directly from the total photoabsorption cross section by Baldin's sum rule [18], which yields a precise value for the sum of the scalar polarizabilities

$$\begin{aligned} \alpha + \beta &= 14.2 \pm 0.5 \quad \text{(Ref. [19])} \\ &= 13.69 \pm 0.14 \quad \text{(Ref. [20])} \ . \end{aligned} \tag{5}$$

Similarly, the forward spin-flip amplitude can be evaluated by an integral over the difference of the absorption cross sections in states with helicity 3/2 and 1/2,

$$\begin{aligned} \gamma_0 = \gamma_1 - \gamma_2 - 2\gamma_4 &= -1.34 \ \text{(Ref. [21])} \\ &= -0.6 \ \text{(Ref. [16])} \ . \end{aligned} \tag{6}$$

While these predictions rely on pion photoproduction multipoles, the helicity cross sections have now been directly determined by scattering photons with circular polarizations on polarized protons [22].

In the case of forward Compton scattering the momentum transfer and, hence, the Mandelstam variable t vanishes. In that sense the above sum rules of Eqs. (5, 6) are derived from DR at $t = 0$. At finite angles, however, the analysis requires DR at $t = \text{const.} \leq 0$, in a range of values between 0 (forward scattering) and the largest negative value of t ($t = t_{\rm max}$), determined by the largest scattering angle at the highest photon energy. As mentioned above, the most quantitative and detailed such analysis has been performed by L'vov and collaborators [5,23] in the framework of unsubtracted DR at $t = \text{const}$. Unfortunately, not all of the dispersion integrals converge, as can be inferred from Regge theory. The reason for the divergence of the integrals is essentially given by fixed poles in the t channel, notably the exchange of the neutral pion and of a somewhat fictitious σ meson with a mass of about 600 MeV and a large width, which models the two-pion continuum with the quantum numbers $I = J = 0$. In a more formal view, the dispersion integral is performed along the real axis in the range $-\nu_{max} \leq \nu \leq +\nu_{max}$, with $\nu_{max} \approx 1.5$ GeV, and then closed by a semi-circle with radius ν_{max} in the upper half of the complex ν-plane. The contribution of the semi-circle is then identified with the asymptotic contribution described by t-channel poles. This introduces unknown vertex functions and the mass of the "σ meson", which have to be determined from the experiment. Moreover, the analysis depends appreciably on the choice of ν_{max}, and there are substantial contributions of intermediate states beyond the relatively well-known pion-nucleon continuum. These higher states include multipion, η- and ρ-meson production, $\Delta\pi$-loops and nonresonant s-wave background. The physics behind these effects is certainly worthwhile studying, and there can be no doubt that within the next years we shall learn more about them by detailed coincidence studies of multipion and heavier meson production, but also directly from a careful analysis of Compton scattering at the higher energies [5]. However, the quest for the polarizabilities as fundamental structure constants should not be burdened by too many open questions and phenomenological models.

In view of the problems of unsubtracted DR, we propose to analyse Compton scattering in the framework of subtracted DR at constant t, with the eventual goal to determine the 6 polarizabilities with the least possible model dependence. We choose to subtract the 6 Compton amplitudes $A_i(\nu, t)$ at the unphysical value $\nu = 0$, i.e. write subtracted DR for $A_i(\nu, t) - A_i(0, t)$ at constant t. As we shall show in the following, these subtracted DR converge nicely and are quite well saturated already at $\nu \approx 400 - 550$ MeV, i.e. essentially by one-pion production. Clearly the price to pay are 6 new functions $A_i(0, t)$, which have to be determined by another set of dispersion relations, at ν=const=0 and by use of information obtained from the t-channel reaction $\gamma\gamma \to$ anything.

In order to reduce the dependence on the higher intermediate states in the t-channel, we subtract again, i.e. write DR for $A_i(0,t) - A_i(0,0)$, the subtraction constants $A_i(0,0)$ being linear combinations of the 6 polarizabilities. Since 4 of these subtraction constants can be calculated from unsubtracted DR at t=const, only 2 parameters have to be fixed by a fit to low energy Compton scattering, the combinations $\alpha - \beta$ and $\gamma_\pi = \gamma_1 + \gamma_2 + 2\gamma_4$ describing the backward non spin-flip and spin-flip amplitudes, respectively.

In a somewhat similar approach, Holstein and Nathan [24] combined s- and t-channel information to predict the backward scalar polarizability $\alpha - \beta$. Using unsubtracted backward DR they obtained, from the integration along the lower boundary of the $s-$channel region, the result $(\alpha - \beta)^s = -6 \pm 3$, and from the t-channel region a contribution of $(\alpha - \beta)^t \approx 9$. The sum of these two contributions, $\alpha - \beta \approx 3 \pm 3$, is at variance with the presently accepted experimental (global average) value, $\alpha - \beta = 10.0 \pm 1.5 \pm 0.9$ of Ref. [4]. The difficulty to predict this observable is due to the bad convergence of the integrals in both the $s-$ and the t-channel regions. As may be seen from Fig. 3 of Ref. [24], the t-channel integral obtains quite sizeable contributions from $10\, m_\pi^2 < t < 40\, m_\pi^2$, in which region the integrand changes its sign. Independent of the numerical analysis, the authors find an extremely interesting relationship connecting the polarizabilities of pions and nucleons. This connection comes via the t-channel integral for the nucleon and the low-energy expansion of the s-wave $\gamma\gamma \to \pi\pi$ amplitude, and results in $\delta\alpha = -\delta\beta = 0.5\alpha^\pi \approx 1.4$, which is the contribution of the pion polarizability α^π to the nucleon's electric and magnetic polarizabilities. In concluding this discussion we point out the difference of our present approach and the calculation of Ref. [24]. We do not intend to predict $\alpha - \beta$. Instead we want to develop a dispersion description of Compton scattering allowing for a derivation of $\alpha - \beta$ with a minimum of model dependence. For this purpose we use a scheme of subtracted DR whose subtraction constants are linear combinations of polarizabilities, which have to be determined by a fit to the Compton data.

In section II we shall give a general introduction to subtracted DR. This technique is then applied to the cases of DR at t=const (s-channel dispersion integral) and DR at $\nu = 0$ (t-channel dispersion integral) in sections III and IV, respectively. Our results are compared to the existing low-energy Compton data in section V, and our conclusions are drawn in section VI.

II. FIXED-T SUBTRACTED DISPERSION RELATIONS

Assuming invariance under parity, charge conjugation and time reversal symmetry, the general amplitude for Compton scattering can be expressed in terms of six independent structure functions $A_i(\nu, t)$, $i = 1, ..., 6$. These structure functions depend on two Lorentz invariant variables, e.g. ν and t as defined in the following. Denoting the momenta of the initial state photon and proton by q and p respectively, and with corresponding final state momenta q' and p', the familiar Mandelstam variables are

$$s = (q+p)^2 \ , \quad t = (q-q')^2 \ , \quad u = (q-p')^2 \ . \tag{7}$$

These variables fulfill the constraint

$$s + t + u = 2M^2 \ . \tag{8}$$

The variable ν is defined by,

$$\nu = \frac{s-u}{4M} = E_\gamma + \frac{t}{4M} \ , \tag{9}$$

where E_γ is the photon energy in the *lab* frame and M the nucleon mass. The Mandelstam plane is shown in Fig. 1, and the boundaries of the physical and spectral regions are discussed in Appendix A.

The invariant amplitudes A_i are free of kinematical singularities and constraints, and because of the crossing symmetry they satisfy the relation $A_i(\nu,t) = A_i(-\nu,t)$. Assuming further analyticity and an appropriate high-energy behavior, the amplitudes A_i fulfill unsubtracted dispersion relations at fixed t,

$$\mathrm{Re}A_i(\nu,t) \ = \ A_i^B(\nu,t) \ + \ \frac{2}{\pi}\,\mathcal{P}\int_{\nu_{thr}}^{+\infty} d\nu' \ \frac{\nu'\ \mathrm{Im}_s A_i(\nu',t)}{\nu'^2-\nu^2} \ , \tag{10}$$

where A_i^B are the Born (nucleon pole) contributions, $\mathrm{Im}_s A_i$ the discontinuities across the s-channel cuts of the Compton process and $\nu_{thr} = m_\pi + (m_\pi^2 + t/2)/(2M)$. However, such unsubtracted dispersion relations require that at high energies ($\nu \to \infty$) the amplitudes $\mathrm{Im}_s A_i(\nu,t)$ drop fast enough so that the integral of Eq. (10) is convergent and the contribution from the semi-circle at infinity can be neglected. For real Compton scattering, Regge theory predicts the following high-energy behavior for $\nu \to \infty$ and fixed t [5]:

$$\begin{aligned} &A_{1,2} \sim \nu^{\alpha(t)} \ , \\ &A_{3,5,6} \sim \nu^{\alpha(t)-2} \ , \qquad A_4 \sim \nu^{\alpha(t)-3} \ , \end{aligned} \tag{11}$$

where $\alpha(t) \lesssim 1$ is the Regge trajectory. In particular we note that the Regge trajectory with the highest intercept, i.e. $\alpha(0) \approx 1.08$, corresponds to soft pomeron exchange. Due to this high energy behavior, the unsubtracted dispersion integral of Eq. (10) diverges for the amplitudes A_1 and A_2. In order to obtain useful results for these two amplitudes, L'vov et al. [5] proposed to close the contour of the integral in Eq. (10) by a semi-circle of finite radius ν_{max} (instead of the usually assumed infinite radius!) in the complex plane, i.e. the real parts of A_1 and A_2 are calculated from the decomposition

$$\mathrm{Re}A_i(\nu,t) \ = \ A_i^B(\nu,t) \ + \ A_i^{int}(\nu,t) \ + \ A_i^{as}(\nu,t) \ , \tag{12}$$

with A_i^{int} the s-channel integral from pion threshold ν_{thr} to a finite upper limit ν_{max},

$$A_i^{int}(\nu,t) \ = \ \frac{2}{\pi}\,\mathcal{P}\int_{\nu_{thr}}^{\nu_{max}} d\nu' \ \frac{\nu'\ \mathrm{Im}_s A_i(\nu',t)}{\nu'^2-\nu^2} \ , \tag{13}$$

and an 'asymptotic contribution' A_i^{as} representing the contribution along the finite semi-circle of radius ν_{max} in the complex plane. In the actual calculations, the s-channel integral is typically evaluated up to a maximum photon energy $E_\gamma = \nu_{max}(t) - t/(4M) \approx 1.5$ GeV, for which the imaginary parts of the amplitudes can be expressed through unitarity by the meson photoproduction amplitudes (mainly 1π and 2π photoproduction) taken from experiment. All contributions from higher energies are then absorbed in the asymptotic term, which is replaced by a finite number of energy independent poles in the t-channel. In

particular the asymptotic part of A_1 is parametrized in Ref. [5] by the exchange of a scalar particle in the t-channel, i.e. an effective "σ meson",

$$A_1^{as}(\nu,t) \approx A_1^{\sigma}(t) \;=\; \frac{F_{\sigma\gamma\gamma}\, g_{\sigma NN}}{t-m_\sigma^2}\;, \tag{14}$$

where m_σ is the "σ meson" mass, and $g_{\sigma NN}$ and $F_{\sigma\gamma\gamma}$ are the couplings of the "σ meson" to the nucleons and photons respectively. The asymptotic part of A_2 is parametrized by the π^0 t-channel pole.

This procedure is relatively save for A_2 because of the dominance of the π^0 pole or triangle anomaly, which is well established both experimentally and on general grounds as Wess-Zumino-Witten term. However, it introduces a considerable model-dependence in the case of A_1. Though "σ mesons" have been repeatedly reported in the past, their properties were never clearly established. Therefore, this particle should be interpreted as a parametrization of the $I=J=0$ part of the two-pion spectrum, which shows up differently in different experiments and hence has been reported with varying masses and widths.

It is therefore the aim of our present contribution to avoid the convergence problem of unsubtracted DR and the phenomenology necessary to determine the asymptotic contribution. The alternative we shall pursue in the following is to consider DR at fixed t that are once subtracted at $\nu=0$,

$$\mathrm{Re}A_i(\nu,t) \;=\; A_i^B(\nu,t) \;+\; \left[A_i(0,t)-A_i^B(0,t)\right] \;+\; \frac{2}{\pi}\,\nu^2\,\mathcal{P}\int_{\nu_{thr}}^{+\infty} d\nu'\,\frac{\mathrm{Im}_s A_i(\nu',t)}{\nu'\,(\nu'^2-\nu^2)}\;. \tag{15}$$

These subtracted DR should converge for all six invariant amplitudes due to the two additional powers of ν' in the denominator, and they are essentially saturated by the πN intermediate states as will be shown in section III. In other words, the lesser known contributions of two and more pions as well as higher continua are small and may be treated reliably by simple models.

The price to pay for this alternative is the appearance of the subtraction functions $A_i(\nu=0,t)$, which have to be determined at some small (negative) value of t. We do this by setting up a once-subtracted DR, this time in the variable t,

$$\begin{aligned} A_i(0,t) \;-\; A_i^B(0,t) = \left[A_i(0,0) \;-\; A_i^B(0,0)\right] \;+\; \left[A_i^{t-pole}(0,t) \;-\; A_i^{t-pole}(0,0)\right] \\ +\; \frac{t}{\pi}\int_{(2m_\pi)^2}^{+\infty} dt'\,\frac{\mathrm{Im}_t A_i(0,t')}{t'\,(t'-t)} \;+\; \frac{t}{\pi}\int_{-\infty}^{a} dt'\,\frac{\mathrm{Im}_t A_i(0,t')}{t'\,(t'-t)}\;, \end{aligned} \tag{16}$$

where $A_i^{t-pole}(0,t)$ represents the contribution of poles in the t-channel, in particular of the π^0 pole in the case of A_2, which is given by

$$A_2^{\pi^0}(0,t) \;=\; \frac{F_{\pi^0\gamma\gamma}\, g_{\pi NN}}{t-m_\pi^2}\;. \tag{17}$$

The coupling $F_{\pi^0\gamma\gamma}$ is determined through the $\pi^0\to\gamma\gamma$ decay as

$$\Gamma\left(\pi^0\to\gamma\gamma\right) \;=\; \frac{1}{64\,\pi}\,m_{\pi^0}^3\,F_{\pi^0\gamma\gamma}^2\;. \tag{18}$$

Using $\Gamma\,(\pi^0 \to \gamma\gamma) = 7.74$ eV [25], one obtains $F_{\pi^0\gamma\gamma}$ = -0.0252 GeV^{-1}, where the sign is in accordance with the $\pi^0\gamma\gamma$ coupling in the chiral limit, given by the Wess-Zumino-Witten effective chiral Lagrangian. The πNN coupling is taken from Ref. [26] : $g^2_{\pi NN}/4\pi = 13.72$. This yields then for the product of the couplings in Eq. (17) : $F_{\pi^0\gamma\gamma}\, g_{\pi NN} \approx$ -0.331 GeV^{-1}.

The imaginary part in the integral from $4m_\pi^2 \to \infty$ in Eq. (16) is saturated by the possible intermediate states for the t-channel process (see Fig. 2), which lead to cuts along the positive t-axis. For values of t below the $K\bar{K}$ threshold, the t-channel discontinuity is dominated by $\pi\pi$ intermediate states. The second integral in Eq. (16) extends from $-\infty$ to a, where $a \,=\, -4\,(m_\pi^2 + 2Mm_\pi) \approx -1.1$ GeV^2 is the boundary of the su spectral region for $\nu = 0$ (see Appendix A for a detailed discussion). As we are interested in evaluating Eq. (16) for small (negative) values of t ($|t| \ll |a|$), the integral from $-\infty$ to a will be highly suppressed by the denominator of the subtracted DR, and can therefore be neglected. Consequently, we shall saturate the subtracted dispersion integrals of Eq. (16) by the contribution of $\pi\pi$ intermediate states, which turns out to be a good approximation for small t. We will show the convergence of the t-channel dispersion integral in section IV and thus verify the quality of the approximation.

The t-dependence of the subtraction functions $A_i(0,t)$ is now determined, and only the subtraction constants $A_i(0,0)$ remain to be fixed. We note that the quantities

$$a_i = A_i(0,0) \;-\; A_i^B(0,0) \tag{19}$$

are directly related to the polarizabilities, which can then be obtained from a fit to the Compton scattering data. For the spin-independent (scalar) polarizabilities α and β, one finds the two combinations

$$\alpha + \beta \;=\; -\frac{1}{2\pi}\,(a_3 \;+\; a_6)\;, \tag{20}$$

$$\alpha - \beta \;=\; -\frac{1}{2\pi}\,a_1\;, \tag{21}$$

which can be determined from forward and backward scattering respectively. Furthermore, the forward combination $\alpha+\beta$ is related to the total absorption spectrum through Baldin's sum rule [18],

$$(\alpha+\beta)_N \;=\; \frac{1}{2\pi^2}\int_{\nu_{thr}}^{\infty} d\nu'\,\frac{\sigma(\gamma N \to X)}{\nu'^2}\;. \tag{22}$$

The 4 spin dependent polarizabilities γ_1 to γ_4 of Ragusa [27] are defined by

$$\gamma_0 \;\equiv\; \gamma_1 - \gamma_2 - 2\gamma_4 \;=\; \frac{1}{2\pi M}\,a_4\;, \tag{23}$$

$$\gamma_{13} \;\equiv\; \gamma_1 + 2\gamma_3 \;=\; -\,\frac{1}{4\pi M}\,(a_5 \;+\; a_6)\;, \tag{24}$$

$$\gamma_{14} \;\equiv\; \gamma_1 - 2\gamma_4 \;=\; \frac{1}{4\pi M}\,(2\,a_4 \;+\; a_5 \;-\; a_6)\;, \tag{25}$$

$$\gamma_\pi \;\equiv\; \gamma_1 + \gamma_2 + 2\gamma_4 \;=\; -\,\frac{1}{2\pi M}\,(a_2 \;+\; a_5)\;, \tag{26}$$

where γ_0 and γ_π are the spin (vector) polarizabilities in the forward and backward directions respectively. Since the π^0 pole contributes to A_2 only, the combinations γ_0, γ_{13} and γ_{14} of

Eqs. (23)-(25) are independent of this pole term [16], and only the backward spin polarizability γ_π is affected by the anomaly.

Although all 6 subtraction constants a_1 to a_6 of Eq. (19) could be used as fit parameters, we shall restrict the fit to the parameters a_1 and a_2, or equivalently to $\alpha - \beta$ and γ_π. The subtraction constants a_4, a_5 and a_6 will be calculated through an unsubtracted sum rule, as derived from Eq. (10),

$$a_{4,5,6} \;=\; \frac{2}{\pi} \int_{\nu_{thr}}^{+\infty} d\nu' \; \frac{\mathrm{Im}_s A_{4,5,6}(\nu', t=0)}{\nu'} \; . \tag{27}$$

The remaining subtraction constant a_3, which is related to $\alpha + \beta$ through Eq. (20), will be fixed through Baldin's sum rule, Eq. (22), using the value obtained in Ref. [20] : $\alpha + \beta = 13.69$.

III. S-CHANNEL DISPERSION INTEGRAL

In this section we describe the calculation of the s-channel contributions, which enter in the once-subtracted dispersion integral of Eq. (15) and in the calculation of subtraction constants a_4, a_5 and a_6 through Eq. (27). The imaginary part of the Compton amplitude due to the s-channel cuts is determined from the scattering amplitudes of photoproduction on the nucleon by the unitarity relation

$$2\,\mathrm{Im}_s\, T_{fi} = \sum_X (2\pi)^4 \delta^4 (P_X - P_i) T^\dagger_{Xf}\, T_{Xi} \; , \tag{28}$$

where the sum runs over all possible states that can be formed in the photon-nucleon reaction. Due to the energy denominator $1/\nu'(\nu'^2 - \nu^2)$ in the subtracted dispersion integrals, the most important contribution is from the πN intermediate states, while mechanisms involving more pions or heavier mesons in the intermediate states are largely suppressed. In our calculation, we evaluate the πN contribution using the multipole amplitudes from the analysis of Hanstein, Drechsel and Tiator [28] at energies $E_\gamma \leq 500$ MeV and at the higher energies we take as input the SAID multipoles (SP98K solution) [29]. The expansion of $\mathrm{Im}_s A_i$ into this set of multipoles is truncated at a maximum angular momentum $j_{max} = l \pm 1/2 = 7/2$, with the exception of the lower energy range ($E_\gamma \leq 400$ MeV) where we use $j_{\max} = 3/2$. The higher partial waves with $j \geq j_{max} + 1$ are evaluated analytically in the one-pion exchange (OPE) approximation. The relevant formulas to implement the calculation are reported in Appendix B and C of Ref. [5].

The multipion intermediate states are approximated by the inelastic decay channels of the πN resonances. In the spirit of Ref. [5] and the more recent work of Ref. [30], we assume that this inelastic contribution follows the helicity structure of the one-pion photoproduction amplitudes. In this approximation, we first calculate the resonant part of the pion photoproduction multipoles using the Breit-Wigner parametrization of Ref. [31], which is then scaled by a suitable factor to include the inelastic decays of the resonances. The resulting contribution to $\mathrm{Im}_s\, A_i$ is

$$[\mathrm{Im}_s\, A_i]^{(N^* \to \pi\pi N, \eta N, \ldots)} = R\, [\mathrm{Im}_s\, A_i]^{(N^* \to \pi N)} \; , \tag{29}$$

with the ratio R given by

$$R = \frac{1 - B_\pi}{B_\pi} \frac{\bar{\Gamma}_{\rm inel}(W)}{\bar{\Gamma}_\pi(W)}. \tag{30}$$

In Eq. (30), B_π is the single-pion branching ratio of the resonance N^* and $\bar{\Gamma}_\pi(W)$ the energy-dependent pionic width [31], while the inelastic width $\bar{\Gamma}_{\rm inel}(W)$ of the decays $N^* \to (\pi\pi N,\, \eta N,\, \pi\pi\pi N, ..)$ is parametrized as in Ref. [5] in order to provide the correct threshold behavior for the resonant two pion contribution.

The πN channel consistently reproduces the measured photoabsorption cross section in the energy range $E_\gamma \leq 500$ MeV, while at the higher energies nonresonant mechanisms should be included in addition to the resonant mechanism to fully describe the multipion channels. In Ref. [5], the non-resonant contribution to the two-pion photoproduction channel was approximately taken into account by calculating the OPE diagram of the $\gamma N \to \pi\Delta$ reaction. The difference between the data and the model for two-pion photoproduction consisting of resonant mechanisms plus the OPE diagram for the nonresonant mechanism, was then fitted in Ref. [5] and attributed to a phenomenological, non-resonant $\gamma N \to \pi\Delta$ s-wave correction term.

A more detailed description of the $\pi\pi N$ channel is clearly worthwile to be undertaken, especially in view of the new two-pion photoproduction data (both unpolarized and polarized) that will be available from MAMI and JLab (CLAS) in the near future. However, for the extraction of the polarizabilities, the strategy followed in this paper is to minimize sensitivity and hence model uncertainty to these higher channels.

We show in Fig. 3 that in the subtracted DR, the sensitivity to the multipion channels is indeed very small. For the unsubtracted DR, on the other hand, the influence of the multipion channels amounts to about 30 % of the amplitude A_2. We furthermore note from Fig. 3 that the subtracted DR are essentially saturated at $\nu \approx 0.4$ GeV and that they only receive a negligible contribution from multipion channels. The importance of the multipion channels is even weaker in the case of the amplitudes A_3 to A_6.

In Table I and II, we show our predictions for the dispersion integral of the spin polarizabilities of the proton and neutron, respectively. We list the separate contribution of the πN channel, HDT(1π), and the total result, HDT, which includes the inelastic resonance channels. The last column shows the values of the dispersion calculation of Ref. [23], which is based on the one-pion multipoles of the SAID-SP97K solution and the model for double-pion production mentioned above. The small differences between the one-pion multipoles of SAID-SP97K and SAID-SP98K at the higher energies are practically negligible for the spin polarizabilities, while the results are very sensitive to the differences between the HDT and SAID analyses. As discussed in Ref. [32], this fact is mainly due to a different behaviour of the E_{0+} partial wave near threshold, giving rise to substantial effects in the case of the forward spin polarizability. While the one-pion contribution from SAID-SP98K is $\gamma_0^p = -1.26$ and $\gamma_0^n = -0.03$, we obtain $\gamma_0^p = -0.75$ and $\gamma_0^n = -0.06$ with the HDT multipoles for $E_\gamma \leq 500$ MeV.

IV. T-CHANNEL DISPERSION INTEGRAL

We next evaluate the t-channel dispersion integral in Eq. (16) from $4m_\pi^2$ to ∞. The kinematics of the t-channel reaction $\gamma\gamma \to N\bar{N}$ is shown in Fig. 4. The subtracted dispersion integral is essentially saturated by the imaginary part of the t-channel amplitude $\gamma\gamma \to N\bar{N}$ due to $\pi\pi$ intermediate states. To calculate this contribution, we have to construct the amplitudes $\gamma\gamma \to \pi\pi$ and $\pi\pi \to N\bar{N}$.

We start with the isospin and helicity structure of the $\gamma\gamma \to \pi\pi$ amplitude, denoted by F. Because of the Bose symmetry of the $\gamma\gamma$ state, only the even isospin values $I = 0$ and 2 are possible. We can express the charged ($\gamma\gamma \to \pi^+\pi^-$) and neutral ($\gamma\gamma \to \pi^0\pi^0$) amplitudes in terms of those with good isospin by

$$\begin{aligned} F^{(\pi^+\pi^-)} &= \sqrt{\frac{2}{3}}\, F^{I=0} + \sqrt{\frac{1}{3}}\, F^{I=2} \quad \text{(charged pions)}\,, \\ F^{(\pi^0\pi^0)} &= -\sqrt{\frac{1}{3}}\, F^{I=0} + \sqrt{\frac{2}{3}}\, F^{I=2} \quad \text{(neutral pions)}\,. \end{aligned} \tag{31}$$

The reaction $\gamma\gamma \to \pi\pi$ has two independent helicity amplitudes $F_{\Lambda_\gamma}(t, \theta_{\pi\pi})$, where $\Lambda_\gamma \equiv \lambda'_\gamma - \lambda_\gamma$, being the difference of the final photon helicity (λ'_γ) and the initial photon helicity (λ_γ), takes on the values 0 or 2, depending upon whether the photons have the same ($\Lambda_\gamma = 0$) or opposite ($\Lambda_\gamma = 2$) helicities. The $\gamma\gamma \to \pi\pi$ helicity amplitudes depend upon the c.m. energy squared t, and the pion c.m. scattering angle $\theta_{\pi\pi}$. In terms of the helicity amplitudes F_{Λ_γ}, the $\gamma\gamma \to \pi\pi$ differential c.m. cross section is given by

$$\left(\frac{d\sigma}{d\cos\theta_{\pi\pi}}\right)_{\rm c.m.} = \frac{\beta}{64\,\pi\,t}\,\left\{|F_{\Lambda_\gamma=0}(t,\theta_{\pi\pi})|^2 + |F_{\Lambda_\gamma=2}(t,\theta_{\pi\pi})|^2\right\}\,, \tag{32}$$

with $\beta = \sqrt{1 - 4m_\pi^2/t}$ the pion velocity. In Appendix B, we give the partial wave expansion of the $\gamma\gamma \to \pi\pi$ helicity amplitudes $F^I_{\Lambda_\gamma}(t, \theta_{\pi\pi})$ for a state of isospin I, and thus define the partial wave amplitudes $F^I_{J\,\Lambda_\gamma}(t)$ (see Eqs. (B10) and (B15)), where J can only take on even values.

To construct the helicity amplitudes F_{Λ_γ} for the process $\gamma\gamma \to \pi\pi$, we first evaluate the Born graphs as shown in Fig. 5. These graphs only contribute to the charged channel $\gamma\gamma \to \pi^+\pi^-$. The Born contributions to the helicity amplitudes $F^{(\pi^+\pi^-)}_{\Lambda_\gamma}$ are denoted as B_{Λ_γ} and given by

$$\begin{aligned} B_{\Lambda_\gamma=0}(t,\theta_{\pi\pi}) &= \left(2e^2\right)\,\frac{1 - \beta^2}{1 - \beta^2\cos^2\theta_{\pi\pi}}\,, \\ B_{\Lambda_\gamma=2}(t,\theta_{\pi\pi}) &= \left(2e^2\right)\,\frac{\beta^2\sin^2\theta_{\pi\pi}}{1 - \beta^2\cos^2\theta_{\pi\pi}}\,. \end{aligned} \tag{33}$$

The partial wave expansion of the Born terms $B_{J\,\Lambda_\gamma}(t)$ is discussed in Appendix B (Eq. (B16)). As the Born amplitudes are only non-zero for the charged pion channel, the two isospin amplitudes of Eq.(31) are related by

$$B^{I=0}_{J\Lambda_\gamma} = \sqrt{\frac{2}{3}}\, B_{J\Lambda_\gamma}\,, \qquad\qquad B^{I=2}_{J\Lambda_\gamma} = \sqrt{\frac{1}{3}}\, B_{J\Lambda_\gamma}\,. \tag{34}$$

We now construct the unitarized amplitudes $F^I_{J\Lambda_\gamma}(t)$, starting from the Born amplitudes $B^I_{J\Lambda_\gamma}(t)$ and following the method outlined in Refs. [33,34]. We first note that the low energy theorem requires for each partial wave that

$$\frac{F^I_{J\Lambda_\gamma}}{B^I_{J\Lambda_\gamma}} \,\rightarrow\, 1\,,\ \text{as}\ \ t \,\rightarrow\, 0\,. \tag{35}$$

Next, the invariant amplitude for the process $\gamma\gamma \,\rightarrow\, \pi\pi$ is assumed to have Mandelstam analyticity. Each partial wave then has a right-hand cut from $t \,=\, 4m_\pi^2$ to $+\infty$ and a left-hand cut from $t \,=\, -\infty$ to 0. Though the Born amplitude is real for all values of t, its partial waves are complex below $t = 0$. The partial waves of the full amplitude have no other sources of complexity in this region, and so we can write a DR for the difference of the full and the Born amplitudes,

$$\frac{F^I_{J\Lambda_\gamma}(t) \,-\, B^I_{J\Lambda_\gamma}(t)}{t(t \,-\, 4m_\pi^2)^{\frac{J}{2}}} \;=\; \frac{1}{\pi}\int_{4m_\pi^2}^{\infty} dt'\, \frac{\mathrm{Im}F^I_{J\Lambda_\gamma}(t')}{t'(t' \,-\, 4m_\pi^2)^{\frac{J}{2}}(t'-t)}\,, \tag{36}$$

with an additional factor of $(t(t \,-\, 4m_\pi^2)^{\frac{J}{2}})^{-1}$ providing the right asymptotics for the convergence of the integral. The next step is to evaluate the imaginary part of the amplitude in Eq. (36). To do this, we exploit the unitarity condition

$$\mathrm{Im}\, F^I_{J\Lambda_\gamma}(\gamma\gamma \,\rightarrow\, \pi\pi) \;=\; \sum_n \rho_n\, F^{I*}_{J\Lambda_\gamma}(\gamma\gamma \,\rightarrow\, n)\, \mathcal{I}^I_J(n \,\rightarrow\, \pi\pi)\,, \tag{37}$$

where ρ_n are the appropriate kinematical and isospin factors for the intermediate channels n, and $\mathcal{I}(n \,\rightarrow\, \pi\pi)$ is a hadronic amplitude. Below the next inelastic threshold, it follows from unitarity that the phase $\phi_J^{I\,(\gamma\gamma\,\rightarrow\,\pi\pi)}$ of each partial wave $F^I_{J\,\Lambda_\gamma}$ is equal to the phase $\delta^{I\,J}_{\pi\pi}$ of the corresponding $\pi\pi \,\rightarrow\, \pi\pi$ partial wave,

$$\begin{aligned} \mathrm{Im}\, F^I_{J\Lambda_\gamma}(\gamma\gamma \,\rightarrow\, \pi\pi) &= \,\rho_{\pi\pi}\, F^{I*}_{J\Lambda_\gamma}(\gamma\gamma \,\rightarrow\, \pi\pi)\, \mathcal{I}^I_J(\pi\pi \,\rightarrow\, \pi\pi) \\ &\Downarrow \\ \phi_J^{I\,(\gamma\gamma\,\rightarrow\,\pi\pi)}(t) &= \,\delta^{IJ}_{\pi\pi}(t)\,. \end{aligned} \tag{38}$$

This fact can be incorporated into the so-called Omnès function, which is constructed to have the phase of the $\pi\pi$ scattering amplitude above $\pi\pi$ threshold, and to be real otherwise,

$$\Omega^I_J(t) \;=\; \exp\left[\frac{t}{\pi}\int_{4m_\pi^2}^{\infty} dt'\, \frac{\delta^{IJ}_{\pi\pi}(t')}{t'(t' \,-\, t \,-\, i\varepsilon)}\right]. \tag{39}$$

The function $F^I_{J\Lambda_\gamma}(\Omega^I_J)^{-1}(t)$ is by construction real above $\pi\pi$ threshold, but complex below threshold due to the complexity of the Born partial waves $B^I_{J\Lambda_\gamma}$. Hence we can write a dispersion relation for $\left[F^I_{J\Lambda_\gamma} \,-\, B^I_{J\Lambda_\gamma}\right](\Omega^I_J)^{-1}(t)/t(t-4m_\pi^2)^{J/2}$,

$$\begin{aligned} &F^I_{J\Lambda_\gamma}(t) \;= \\ &\Omega^I_J(t)\,\left\{B^I_{J\Lambda_\gamma}(t)\,\mathrm{Re}\left[(\Omega^I_J)^{-1}(t)\right] \,-\, \frac{t(t \,-\, 4m_\pi^2)^{J/2}}{\pi}\int_{4m_\pi^2}^{\infty} dt'\, \frac{B^I_{J\Lambda_\gamma}(t')\,\mathrm{Im}\left[(\Omega^I_J)^{-1}(t')\right]}{t'(t' \,-\, 4m_\pi^2)^{J/2}(t' \,-\, t)}\right\}\,. \end{aligned} \tag{40}$$

For $t > 4m_\pi^2$, this integral is understood to be a principal value integral, which we implement by subtracting the integrand at $t' = t$. In this way we obtain a regular integral, which can be performed without numerical problems,

$$F^I_{J\Lambda_\gamma}(t) \;=\; \Omega^I_J(t)\,\left\{B^I_{J\Lambda_\gamma}(t)\,\left(\mathrm{Re}\big[(\Omega^I_J)^{-1}(t)\big] \;+\; \mathrm{Im}\big[(\Omega^I_J)^{-1}(t)\big]\;\frac{1}{\pi}\;\ln(\frac{t}{4m_\pi^2}\;-1\,)\right)\right.$$
$$\left. -\;\frac{t(t\;-\;4m_\pi^2)^{J/2}}{\pi}\int_{4m_\pi^2}^{\infty}\frac{dt'}{t'(t'-t)}\;\left(\frac{B^I_{J\Lambda_\gamma}(t')\,\mathrm{Im}\big[(\Omega^I_J)^{-1}(t')\big]}{(t'\;-\;4m_\pi^2)^{J/2}}\;-\;\frac{B^I_{J\Lambda_\gamma}(t)\,\mathrm{Im}\big[(\Omega^I_J)^{-1}(t)\big]}{(t\;-\;4m_\pi^2)^{J/2}}\right)\right\}\;. \quad (41)$$

In our formalism, the s($J = 0$)- and d($J = 2$)-waves are unitarized. For the s- and d-wave $\pi\pi$ phaseshifts, we use the solutions that were determined in Ref. [35]. For the higher partial waves, the corresponding $\pi\pi$ phaseshifts are rather small and are not known with good precision. Therefore, we will approximate all higher partial waves ($J \geq 4$) by their Born contribution. The full amplitudes for the charged and neutral channels can then be cast into the forms

$$F^{(\pi^+\pi^-)}_{\Lambda_\gamma}(t,\theta_{\pi\pi}) \;=\; B_{\Lambda_\gamma}(t,\theta_{\pi\pi})$$
$$+\;\sum_{J=0,2}\sqrt{2J+1}\sqrt{\frac{(J-\Lambda_\gamma)!}{(J+\Lambda_\gamma)!}}\left[\sqrt{\frac{2}{3}}F^{I=0}_{J\Lambda_\gamma}(t)\;+\;\sqrt{\frac{1}{3}}F^{I=2}_{J\Lambda_\gamma}(t)\;-\;B_{J\Lambda_\gamma}(t)\right]P_J^{\Lambda_\gamma}(\cos\theta_{\pi\pi})\;, \quad (42)$$

$$F^{(\pi^0\pi^0)}_{\Lambda_\gamma}(t,\theta_{\pi\pi}) \;=\; \sum_{J=0,2}\sqrt{2J+1}\sqrt{\frac{(J-\Lambda_\gamma)!}{(J+\Lambda_\gamma)!}}\left[-\sqrt{\frac{1}{3}}F^{I=0}_{J\Lambda_\gamma}(t)\;+\;\sqrt{\frac{2}{3}}F^{I=2}_{J\Lambda_\gamma}(t)\right]P_J^{\Lambda_\gamma}(\cos\theta_{\pi\pi})\;. \quad (43)$$

The two-pion intermediate contribution holds to good precision up to $K\bar{K}$ threshold (≈ 1 GeV^2), because the four-pion intermediate state couples only weakly and gives only small inelasticities in the $\pi\pi$ phaseshifts.

In Figs. 6 and 7, we show our results for the total and differential $\gamma\gamma \to \pi^+\pi^-$ cross sections and a comparison to the existing data. In the threshold region, the charged pion cross sections are clearly dominated by the Born graphs of Fig. 5 because of the vicinity of the pion pole in the t-channel of the $\gamma\gamma \to \pi^+\pi^-$ process. However, the results for the unitarized calculation show that s-wave rescattering is not negligible but leads to a considerable enhancement at energies just above threshold. Besides the low energy structure, driven by the Born terms, the $\gamma\gamma \to \pi\pi$ process has a prominent resonance structure at higher energies corresponding to excitation of the isoscalar $f_2(1270)$ resonance, with mass $m_{f_2} = 1275$ MeV and width $\Gamma_{f_2} = 185.5$ MeV [25]. The f_2 resonance shows up in the partial wave $F_{J=2\,\Lambda_\gamma=2}$ as outlined in Appendix C. Therefore, the most efficient way to unitarize this particular partial wave is to make a Breit-Wigner ansatz for the f_2 excitation, which is described in Appendix C where we also give some details of the formalism for a spin-2 particle. The Breit-Wigner ansatz for the f_2 contribution to the partial wave $F_{J=2\,\Lambda_\gamma=2}$ depends upon the couplings $f_2\pi\pi$ and $f_2\gamma\gamma$. The coupling $f_2\pi\pi$ is known from the decay $f_2 \to \pi\pi$ and is taken from Ref. [25]. The coupling $f_2\gamma\gamma$ is then fitted to the $\gamma\gamma \to \pi\pi$ cross section at the f_2 resonance position, and is consistent with the value quoted in Ref. [25]. The resulting amplitude, consisting of unitarized s-wave, f_2 excitation and Born terms for all other partial waves (with $J \geq 4$) is seen from Figs. 6 and 7 to give a rather good description of the

$\gamma\gamma \to \pi^+\pi^-$ data up to $W_{\pi\pi} \simeq 1.8$ GeV. Only in the region $W_{\pi\pi} \approx 0.7$ - 0.8 GeV, does our description slightly overestimate the data.

Having constructed the $\gamma\gamma \to \pi\pi$ amplitudes, we next need the $\pi\pi \to N\bar{N}$ amplitudes in order to estimate the contribution of the $\pi\pi$ states to the t-channel dispersion integral for Compton scattering. As we only kept s- and d-waves for $\gamma\gamma \to \pi\pi$, we will only need the s- and d-waves ($J = 0,\ 2$) for $\pi\pi \to N\bar{N}$. For every partial wave J, there are two independent $\pi\pi \to N\bar{N}$ helicity amplitudes $f^J_\pm(t)$, depending on whether the nucleon and anti-nucleon have the same ($f^J_+(t)$) or opposite ($f^J_-(t)$) helicities. We refer the reader to Appendix B (Eqs. (B11) and (B13)) for details. In this work, we take the s- and d-waves from the work of Höhler and collaborators [36], in which the lowest $\pi\pi \to N\bar{N}$ partial wave amplitudes were constructed from a partial wave solution of pion-nucleon scattering, by use of the $\pi\pi$ phaseshifts of Ref. [35], which we also used to construct the $\gamma\gamma \to \pi\pi$ amplitudes. In Ref. [36], the $\pi\pi \to N\bar{N}$ amplitudes are given for t values up to $t \approx 40 \cdot m_\pi^2 \approx 0.78$ GeV^2, which will serve well for our purpose since the subtracted t-channel dispersion integral will have converged much below this value as shown in the following.

Finally, we can now combine the $\gamma\gamma \to \pi\pi$ and $\pi\pi \to N\bar{N}$ amplitudes to construct the discontinuities of the Compton amplitudes across the t-channel cut. In Appendix B, we show in detail how the Compton invariant amplitudes $A_1, ..., A_6$ are expressed by the t-channel ($\gamma\gamma \to N\bar{N}$) helicity amplitudes. Through unitarity we then express the imaginary parts of these t-channel ($\gamma\gamma \to N\bar{N}$) helicity amplitudes in terms of the $\gamma\gamma \to \pi\pi$ and $\pi\pi \to N\bar{N}$ amplitudes. We finally express the discontinuities $\mathrm{Im}_t A_i$ of the invariant amplitudes A_i (i = 1,...,6) in terms of the corresponding $\gamma\gamma \to \pi\pi$ and $\pi\pi \to N\bar{N}$ partial wave amplitudes (see Eq. (B17)). As we restrict ourselves to s- and d-wave intermediate states in the actual calculations, we give here the expressions at $\nu = 0$, including s- and d-waves only, that are needed for the subtracted t-channel dispersion integral of Eq. (16) ,

$$
\begin{aligned}
\mathrm{Im}_t A_1(\nu=0,t)^{2\pi} &= -\sqrt{\frac{t/4-m_\pi^2}{t}}\,\frac{1}{t\,(M^2-t/4)}\,F_{0\,\Lambda_\gamma=0}(t)\,f_+^{0*}(t) \\
&\quad -\left(\frac{t/4-m_\pi^2}{t}\right)^{3/2}\,\frac{\sqrt{5}}{2}\,F_{2\,\Lambda_\gamma=0}(t)\,f_+^{2*}(t)\,, \\
\mathrm{Im}_t A_2(\nu=0,t)^{2\pi} &= 0\,, \\
\mathrm{Im}_t A_3(\nu=0,t)^{2\pi} &= -\left(\frac{t/4-m_\pi^2}{t}\right)^{3/2}\,\frac{M^2}{(M^2-t/4)}\,\frac{\sqrt{5}}{2}\,F_{2\,\Lambda_\gamma=2}(t)\,\left\{\sqrt{\frac{3}{2}}\,f_+^{2*}(t)\,-\,M\,f_-^{2*}(t)\right\}\,, \\
\mathrm{Im}_t A_4(\nu=0,t)^{2\pi} &= 0\,, \\
\mathrm{Im}_t A_5(\nu=0,t)^{2\pi} &= -\left(\frac{t/4-m_\pi^2}{t}\right)^{3/2}\,M\,\sqrt{\frac{15}{2}}\,F_{2\,\Lambda_\gamma=0}(t)\,f_-^{2*}(t)\,, \\
\mathrm{Im}_t A_6(\nu=0,t)^{2\pi} &= -\left(\frac{t/4-m_\pi^2}{t}\right)^{3/2}\,M\,\frac{\sqrt{5}}{2}\,F_{2\,\Lambda_\gamma=2}(t)\,f_-^{2*}(t)\,. \qquad (44)
\end{aligned}
$$

The reader should note that the s-wave $\pi\pi$ intermediate state only contributes to the amplitude A_1. It is the t-dependence of this $I = J = 0$ $\pi\pi$ state in the t-channel that is approximated in Ref. [5] and parametrized by a "sigma" pole. The d-wave $\pi\pi$ intermediate state gives rise to imaginary parts for the amplitudes A_1, A_3, A_5 and A_6. The amplitude A_2 (at $\nu = 0$) corresponds to the t-channel exchange of an object with the quantum numbers

of the pion (e.g. π^0 pole in Eq. (17)). Therefore two-pion intermediate states do not have the quantum numbers to contribute to the amplitude A_2. The imaginary part of A_4 receives only contributions from $\pi\pi$ intermediate states with $J \geq 4$ (see Eq. (B17)) and therefore is zero in our description, as we keep only s- and d-waves.

In Fig. 8 we show the convergence of the t-channel integral from $4m_\pi^2$ to ∞ in the subtracted DR of Eq. (16). We do so by calculating the dispersion integral as function of the upper integration limit $t_{\rm upper}$ and by showing the ratio with the integral for $t_{\rm upper} = 0.78$ GeV^2. The latter value corresponds to the highest t value for which the $\pi\pi \to N\bar{N}$ amplitudes are given in Ref. [36]. One clearly sees from Fig. 8 that the unsubtracted t-channel DR shows only a slow convergence, whereas the subtracted t-channel DR has already reached its final value, within the percent level, at a t value as low as 0.4 GeV^2.

V. RESULTS AND DISCUSSION

In this section we shall present our results for Compton scattering off the nucleon in the dispersion formalism presented above.

The real and imaginary parts of the six Compton amplitudes are displayed in Fig. 9. Note that for the real part, we only show the subtracted s-channel integral of Eq. (15). As can be seen from Fig. 9, these amplitudes show strong oscillations due to interference effects between different pion photoproduction multipoles, in particular for threshold pion production by E_{0+} and Δ-excitation by M_{1+}.

In Figs. 10 and 11 we show our predictions in the subtracted DR formalism and compare them with the available Compton data on the proton below pion threshold. These data were used in Ref. [4] to determine the scalar polarizabilities α and β through a global fit, with the results given in Eq. (1). In the analysis of Ref. [4], the unsubtracted DR formalism was used and the asymptotic contributions (Eq. (12)) to the invariant Compton amplitudes A_1 and A_2 were parametrized. In particular, A_2^{as} was described by the π^0 pole, which yields the value $\gamma_\pi \simeq -45$. The free parameter entering in A_1^{as} was related to $\alpha - \beta$, for which the fit obtained the value $\alpha - \beta \simeq 10$. Keeping $\alpha - \beta$ fixed at that value, we demonstrate in Fig. 10 that the sensitivity to γ_π is not at all negligible, especially at the backward angles and the higher energies. Although we do not intend to give a best fit at the present stage, the subtracted DR formalism allows one to directly use the values $\alpha - \beta$ and γ_π as fit parameters, as is obvious from Eqs. (15, 16). We investigate this further in Fig. 11, where we show our results for different $\alpha - \beta$ and for a fixed value of $\gamma_\pi = -37$, which is consistent with the heavy baryon ChPT prediction [14] and close to the value obtained in Ref. [17] in a backward DR formalism. For that value of γ_π, a better description of the data (in particular at the backward angle) seems to be possible by using a smaller value for $\alpha - \beta$ than determined in Ref. [4]. For a more reliable extraction of the polarizabilities, more accurate data over the whole angular and energy range are necessary. Recently, Compton data were taken at MAMI over a wide angular range below pion threshold [37]. It will be interesting to perform a best fit for $\alpha - \beta$ and γ_π with such an extended data base.

As one moves to energies above pion threshold, the Compton cross section rises rapidly because of the unitarity coupling to the much stronger pion photoproduction channel. Therefore this higher energy region is usually considered less 'pure' to extract polarizabilities because the procedure would require a rather precise knowledge of pion photoproduction.

With the quite accurate pion photoproduction data on the proton that have become available in recent years, the energy region above pion threshold for the Compton channel could however serve as a valuable complement to determine the polarizabilities, provided one can minimize the model uncertainties in the dispersion formalism. In this work, we use the most recent information on the pion photoproduction channel by taking the HDT [28] multipoles at energies $E_\gamma \leq 500$ MeV and the SAID-SP98K solution [29] at higher energies. In addition, as previously shown in Fig. 3, the subtracted dispersion relations are practically saturated by the one-pion channel for photon energies through the Δ region, which minimizes the uncertainty due to the modeling of the two-pion photoproduction channels. In Figs. 12 and 13 we display the sensitivity of the Compton cross sections to γ_π and $\alpha - \beta$ in the lower part of the Δ region in comparison with the available data. As can be seen from Fig. 12, these data are quite sensitive to the backward spin polarizability γ_π. This sensitivity was exploited in Ref. [8] within the context of an unsubtracted DR formalism, and the value $\gamma_\pi \simeq -27$ was extracted from the LEGS 97 data, which are shown at the higher energies in Fig. 12. Our results for the subtracted DR are obtained in Fig. 12 by variation of γ_π at fixed $\alpha - \beta =$ 10, and by variation of $\alpha - \beta$ at fixed γ_π = -37 in Fig. 13. For γ_π we show the results for values between $\gamma_\pi = -27$ and $\gamma_\pi = -37$. One sees that the lower energy data ($E_\gamma = 149$ MeV and 182 MeV) can be easily described by the larger values of γ_π if $\alpha - \beta$ decreases to some value below 10. On the other hand, the higher energy data ($E_\gamma = 230$ MeV and 287 MeV) seem to favor a smaller value of γ_π, and so far we confirm the conclusion reached in Ref. [8]. However, we have to point out that, at these higher energies, the data around 90^o cannot be described in our subtracted DR formalism for reasonable values of $\alpha - \beta$ and γ_π.

This is also seen in Fig. 14 at two fixed angles, now as function of the energy throughout the Δ resonance region, for the MAMI data at 75^o [7] and 90^o [6]. It is again obvious at these angles that the sensitivity to γ_π is quite small. Therefore the physics of these data is basically driven by pion photoproduction. With the multipoles used here, the 75^o data are well described, but our prediction falls below the 90^o data on the left shoulder of the Δ resonance. In the same energy region there exist also both differential cross section and photon asymmetry data from LEGS [38] by use of the laser backscattering technique. In Fig. 15 we compare our predictions with these data. One finds that at both energies (E_γ = 265 MeV and 323 MeV) our subtracted DR formalism provides a good description of the asymmetries which display only little sensitivity on γ_π, but underestimates the absolute values of the cross sections. In particular close to the resonance position at $E_\gamma = 323$ MeV, the subtracted DR formalism does not allow us to find any reasonable combination of γ_π and $\alpha - \beta$ to describe these data. Therefore, within the present subtracted DR formalism, the actual data situation at these higher energies does not seem to be conclusive to reliably decide on a value of γ_π. Since the uncertainties due to two-pion and heavier meson photoproduction are less than 1 % in our subtracted DR formalism, the only possibility to describe the $E_\gamma =$ 323 MeV LEGS data would be an increase of the HDT M_{1+} multipole by about 2.5 % (see the dotted lines in Fig. 15). Indeed such a fit was obtained by Tonnison et al. [8] by use of the LEGS pion photoproduction multipole set of Ref. [38] for photon energies between 200 and 350 MeV and the SAID-SM95 multipole solution [29] outside this interval. However the more recent SAID-SP98K solution is in very close agreement with the HDT multipoles in the Δ region and hence the predictions also fall below the data at 323 MeV in Fig. 15.

Before coming to any conclusions, we like to point out that new Compton data on the

proton in and above the Δ-resonance region and over a wide angular range have been measured recently at MAMI and reported preliminary [39]. These new data will be most valuable to check if a systematic and consistent trend becomes visible between the data sets at the lower energies and in the Δ region.

Finally, in Fig. 16 we show that double polarization observables will be ultimately necessary in order to reliably extract the polarizabilities $\alpha-\beta$ and γ_π. In particular, an experiment with a circularly polarized photon and a polarized proton target displays quite some sensitivity on the backward spin polarizability γ_π, especially at the somewhat higher energies of $E_\gamma \approx 230$ MeV. Such a measurement is more selective to γ_π due to a lesser sensitivity to $\alpha - \beta$ (see Fig. 16). It will be indeed a prerequisite to disentangle the scalar and vector polarizabilities of the nucleon.

VI. CONCLUSIONS

In this work we have presented a formalism of fixed-t subtracted dispersion relations for Compton scattering off the nucleon at energies $E_\gamma \leq 500$ MeV. Due to the subtraction, the s-channel dispersion integrals converge very fast and are practically saturated by the πN intermediate states. Because of the use of subtracted DR we have minimized the uncertainty from multi-pion and heavier meson intermediate states. Hence this formalism provides a direct cross-check between Compton scattering and one-pion photoproduction. We have described this dominant $\gamma N \to \pi N \to \gamma N$ contribution by using the recent pion photoproduction multipoles of HDT.

To calculate the functional dependence of the subtraction functions on the momentum transfer t, we have included experimental information on the t-channel process through $\pi\pi$ intermediate states as $\gamma\gamma \to \pi\pi \to N\bar{N}$. We have constructed a unitarized amplitude for the $\gamma\gamma \to \pi\pi$ subprocess and found a good description of available data. In this way, we have largely avoided the uncertainties in Compton scattering associated with the two-pion continuum in the t-channel, which was often modeled through the exchange of a somewhat fictitious σ-meson.

As the polarizabilities directly enter as subtraction constants in the subtracted DR formalism, it can be used to extract the nucleon polarizabilities from data with a minimum of model dependence. We have demonstrated the sensitivity to the polarizabilities $\alpha - \beta$ and γ_π of existing Compton data on the proton both below pion threshold as well as in the Δ resonance region. The effects of the polarizabilities $\alpha - \beta$ and γ_π on the Compton cross sections are strongly correlated. Hence these polarizabilities can only be determined simultaneously from unpolarized observables even below pion threshold. When comparing the subtracted DR formalism with the existing data in the Δ resonance region, we have found that the actual data situation at these higher energies does not seem to be conclusive to reliably decide on a value for γ_π. However new Compton data on the proton both below pion threshold and in the Δ region are actually under analysis and will extend considerably the experimental data base to fit the proton polarizabilities.

We have also argued that double polarization observables will ultimately be necessary to extract reliably $\alpha - \beta$ and γ_π. In particular we have shown that experiments of polarized photons on polarized protons show rather large sensitivity to γ_π at energies around $E_\gamma \approx$ 230 MeV and at backward angles. Therefore such polarization experiments hold the promise

to disentangle scalar and vector polarizabilities of the nucleon and to quantify the nucleon spin response in an external electromagnetic field.

ACKNOWLEDGMENTS

The authors are grateful to G. Krein, A. L'vov and members of the A2-Collaboration, in particular J. Ahrens and V. Olmos de Léon, for useful discussions. This work was supported by the Deutsche Forschungsgemeinschaft (SFB 443) and in part by the Marie Curie TMR program (contract ERBFMBICT972758).

APPENDIX A: THE MANDELSTAM PLANE – PHYSICAL AND SPECTRAL REGIONS FOR COMPTON SCATTERING

The kinematics of Compton scattering, $\gamma(q)N(p) \to \gamma(q')N(p')$, can be described in terms of the familiar Mandelstam variables,

$$s = (q+p)^2 \ , \quad t = (q-q')^2 \ , \quad u = (q-p')^2 \ , \tag{A1}$$

with the constraint

$$s + t + u = 2M^2 \ . \tag{A2}$$

Furthermore we introduce the coordinate ν perpendicular to t,

$$\nu = \frac{s-u}{4M} = E_\gamma + \frac{t}{4M} \ . \tag{A3}$$

In these equations, E_γ is the photon energy in the *lab* frame and M the nucleon mass.

The boundaries of the physical regions in the s, u and t channels are determined by the zeros of the Kibble function Φ,

$$\Phi(s,t,u) = t(us - M^4) = 0 \ . \tag{A4}$$

The 3 physical regions are shown by the horizontally hatched areas in Fig. 1. The vertically hatched areas are the regions of non-vanishing double spectral functions. These spectral regions are those regions in the Mandelstam plane where two of the three variables s, t and u take on values that correspond with a physical (i.e. on-shell) intermediate state. The boundaries of these regions follow from unitarity. As discussed in Ref. [36], it is sufficient to consider two-particle intermediate states in all channels. Since these boundaries depend only on the masses, they are the same for all 6 amplitudes A_i. In the Mandelstam diagram of Fig. 1 they are symmetric to the line $\nu = 0$ due to crossing symmetry. For the spectral function ρ_{su} we obtain the boundary

$$b_I(u,s) = b_I(s,u) = [s - (M+m_\pi)^2][u - (M+m_\pi)^2] - (m_\pi^2 + 2\,M\,m_\pi)^2 = 0 \ , \tag{A5}$$

and for the spectral function ρ_{st} we find

$$b_{II}(s,t) = (t - 4m_\pi^2)[s - (M+m_\pi)^2][s - (M-m_\pi)^2] - 8m_\pi^4(s + M^2 - m_\pi^2/2) = 0 \tag{A6}$$

The boundary of the spectral function ρ_{ut} follows from crossing symmetry. We also note that these boundaries are obtained for the isovector photon, which couples to a $\pi^+\pi^-$ pair. The corresponding boundaries for the isoscalar photon are inside the boundaries of Eqs. (A5) and (A6), because it couples to 3 pions.

APPENDIX B: T-CHANNEL HELICITY AMPLITUDES FOR COMPTON SCATTERING

The t-channel helicity amplitudes for Compton scattering can be expressed in the orthogonal basis of Prange [40] in the following form:

$$T^t_{\lambda_N\lambda_{\bar N},\lambda'_\gamma\lambda_\gamma}(\nu,t) \;=\; (-1)^{\frac{1}{2}-\lambda_{\bar N}}\;\varepsilon'_\mu(q',\lambda'_\gamma)\,\varepsilon_\nu(q,\lambda_\gamma)$$
$$\times\,\bar u(\vec p\,',\lambda_N)\left\{-\frac{\tilde P'^\mu\,\tilde P'^\nu}{\tilde P'^2}\,\left(T_1+\tilde{\not K}T_2\right)\right.$$
$$-\frac{\tilde N^\mu\,\tilde N^\nu}{\tilde N^2}\,\left(T_3+\tilde{\not K}T_4\right)$$
$$+i\,\frac{\tilde P'^\mu\tilde N^\nu-\tilde P'^\nu\tilde N^\mu}{\tilde P'^2\,\tilde K^2}\,\gamma_5\,T_5$$
$$\left.+i\,\frac{\tilde P'^\mu\tilde N^\nu+\tilde P'^\nu\tilde N^\mu}{\tilde P'^2\,\tilde K^2}\,\gamma_5\,\tilde{\not K}T_6\right\}\;v(-\vec p,\lambda_{\bar N})\;, \tag{B1}$$

where

$$\tilde P'^\mu=\tilde P^\mu-\tilde K^\mu\,\frac{\tilde P\cdot\tilde K}{\tilde K^2}\;,\quad \tilde P=\frac{1}{2}\,(-p+p')\;,\quad \tilde K=\frac{1}{2}\,(q-q'),$$
$$\tilde N^\mu=\epsilon^{\mu\alpha\beta\gamma}\,\tilde P'_\alpha\,\tilde Q_\beta\,\tilde K_\gamma\;,\quad \tilde Q=\frac{1}{2}\,(-p-p')=\frac{1}{2}\,(-q'-q)\,, \tag{B2}$$

and using the convention $\epsilon_{0123}=+1$.

In the c.m. system of the t-channel process $\gamma\gamma\to N\bar N$ (see Fig. 4 for the kinematics), we choose the photon momentum $\vec q_t$ (helicity λ'_γ) to point in the z-direction and the nucleon momentum $\vec p\,'=\vec p_t$ in the xz plane at an angle θ_t with respect to the z-axis (the anti-nucleon momentum is then given by $-\vec p=-\vec p_t$). In this frame, the helicity amplitudes of Eq.(B1) can be cast into the form

$$T^t_{\lambda_N\lambda_{\bar N},\lambda'_\gamma\lambda_\gamma}(\nu,t) \;=\; (-1)^{\frac{1}{2}-\lambda_{\bar N}}\;\bar u(\vec p_t,\lambda_N)\left\{-\frac{1}{2}\,\lambda'_\gamma\lambda_\gamma\,\left(T_1+|\vec q_t|\,\gamma^3\,T_2\right)\right.$$
$$-\frac{1}{2}\,\left(T_3+|\vec q_t|\,\gamma^3\,T_4\right)$$
$$-\frac{1}{2}\,(\lambda'_\gamma+\lambda_\gamma)\,\gamma_5\,T_5$$
$$\left.-\frac{1}{2}\,(\lambda'_\gamma-\lambda_\gamma)\,\gamma_5\,|\vec q_t|\,\gamma^3\,T_6\right\}\;v(-\vec p_t,\lambda_{\bar N}). \tag{B3}$$

Under parity transformation, these amplitudes behave as

$$T^t_{\lambda_N\lambda_{\bar N},\lambda'_\gamma\lambda_\gamma}(\nu,t) \;=\; (-1)^{\Lambda_N-\Lambda_\gamma}\;T^t_{-\lambda_N-\lambda_{\bar N},-\lambda'_\gamma-\lambda_\gamma}(\nu,t)\;, \tag{B4}$$

with the helicity differences Λ_γ and Λ_N given by $\Lambda_\gamma=\lambda'_\gamma-\lambda_\gamma$ (with $\Lambda_\gamma=0$ or 2) and $\Lambda_N=\lambda_N-\lambda_{\bar N}$ (with $\Lambda_N=0$ or 1) respectively.

However, the invariant amplitudes $T_i(i=1,...,6)$ of Prange have the disadvantage to behave differently under $s\leftrightarrow u$ crossing. While T_1, T_3, T_5 and T_6 are even functions of ν, T_2 and T_4 are odd functions (note that $\nu\to-\nu$ is equivalent to $s\leftrightarrow u$). Therefore, L'vov used a new set of invariant amplitudes $A_i(i=1,...,6)$, which are all even functions of ν and at the same time free of kinematical singularities [5]

$$
\begin{aligned}
A_1 &= \frac{1}{t}\ \left[T_1\ +\ T_3\ +\ \nu\,(T_2\ +\ T_4)\right]\ ,\\
A_2 &= \frac{1}{t}\ \left[2\,T_5\ +\ \nu\,(T_2\ +\ T_4)\right]\ ,\\
A_3 &= \frac{M^2}{M^4-su}\ \left[T_1\ -\ T_3\ -\ \frac{t}{4\nu}\,(T_2\ -\ T_4)\right]\ ,\\
A_4 &= \frac{M^2}{M^4-su}\ \left[2\,M\,T_6\ -\ \frac{t}{4\nu}\,(T_2\ -\ T_4)\right]\ ,\\
A_5 &= \frac{1}{4\nu}\ \left[T_2\ +\ T_4\right]\ ,\\
A_6 &= \frac{1}{4\nu}\ \left[T_2\ -\ T_4\right]\ .
\end{aligned}
\tag{B5}
$$

In terms of the t-channel helicity amplitudes $T^t_{\lambda_N\lambda_{\bar N},\,\lambda'_\gamma\lambda_\gamma}(\nu,t)$ of Eq. (B1) the invariant amplitudes $A_i(\nu,t)$ (i = 1,...,6) of Eq. (B5) read

$$
\begin{aligned}
A_1 &= \frac{1}{t\,\sqrt{t-4M^2}}\left\{\ \left[T^t_{\frac12\,\frac12,1\,1}\ +\ T^t_{\frac12\,\frac12,-1\,-1}\right]\ -\ \frac{2\,\nu\,\sqrt{t}}{\sqrt{su-M^4}}\ T^t_{\frac12\,-\frac12,1\,1}\right\}\ ,\\
A_2 &= \frac{1}{t\,\sqrt{t}}\left\{\ -\left[T^t_{\frac12\,\frac12,1\,1}\ -\ T^t_{\frac12\,\frac12,-1\,-1}\right]\ -\ \frac{2\,\nu\,\sqrt{t-4M^2}}{\sqrt{su-M^4}}\ T^t_{\frac12\,-\frac12,1\,1}\right\}\ ,\\
A_3 &= \frac{M^2}{su-M^4}\ \frac{1}{\sqrt{t-4M^2}}\left\{\ 2\ T^t_{\frac12\,\frac12,1\,-1}\ +\ \frac{\sqrt{su-M^4}}{\nu\,\sqrt{t}}\ \left[T^t_{\frac12\,-\frac12,1\,-1}\ +\ T^t_{\frac12\,-\frac12,-1\,1}\right]\right\}\ ,\\
A_4 &= \frac{M^2}{su-M^4}\ \frac{1}{\sqrt{su-M^4}}\left\{\ M\left[-\ T^t_{\frac12\,-\frac12,1\,-1}\ +\ T^t_{\frac12\,-\frac12,-1\,1}\right]\right.\\
&\qquad\qquad\left.+\ \frac{\sqrt{t}\,\sqrt{t-4M^2}}{4\,\nu}\ \left[T^t_{\frac12\,-\frac12,1\,-1}\ +\ T^t_{\frac12\,-\frac12,-1\,1}\right]\right\}\ ,\\
A_5 &= \frac{\sqrt{t-4M^2}}{4\,\nu\,\sqrt{t}\,\sqrt{su-M^4}}\left\{\ -2\ T^t_{\frac12\,-\frac12,1\,1}\right\}\ ,\\
A_6 &= \frac{\sqrt{t-4M^2}}{4\,\nu\,\sqrt{t}\,\sqrt{su-M^4}}\left\{\ \left[T^t_{\frac12\,-\frac12,1\,-1}\ +\ T^t_{\frac12\,-\frac12,-1\,1}\right]\right\}\ .
\end{aligned}
\tag{B6}
$$

In the subtracted DR of Eq. (16), the t-channel integral runs along the line $\nu = 0$. Therefore, we have to determine the imaginary parts $\mathrm{Im}_t A_i(\nu=0,t)$ of the invariant amplitudes of Eq. (B6). We start by decomposing of the t-channel helicity amplitudes for $\gamma\gamma \to N\bar N$ into a partial wave series,

$$
T^t_{\lambda_N\lambda_{\bar N},\,\lambda'_\gamma\lambda_\gamma}(\nu,t)\ =\ \sum_J \frac{2J+1}{2}\ T^J_{\lambda_N\lambda_{\bar N},\,\lambda'_\gamma\lambda_\gamma}(t)\ d^J_{\Lambda_N\Lambda_\gamma}(\theta_t)\ ,
\tag{B7}
$$

where $d^J_{\Lambda_N\Lambda_\gamma}$ are Wigner d-functions and θ_t is the scattering angle in the t-channel, which is related to the invariants ν and t by

$$
\cos\theta_t = \frac{4\,M\,\nu}{\sqrt{t}\,\sqrt{t-4M^2}}\ .
\tag{B8}
$$

It is obvious from this equation that $\nu = 0$ corresponds to 90^o scattering for the t-channel process. As explained in Section IV, we calculate the imaginary parts of the t-channel helicity amplitudes $T^t_{\lambda_N \lambda_{\bar{N}}, \lambda'_\gamma \lambda_\gamma}(\nu, t)$ through the unitarity equation by inserting $\pi\pi$ intermediate states, which should give the dominant contribution below $K\bar{K}$ threshold,

$$2\,\mathrm{Im}T_{\gamma\gamma\to N\bar{N}} \;=\; \frac{1}{(4\pi)^2}\,\frac{|\vec{p}_\pi|}{\sqrt{t}}\,\int d\Omega_\pi\;[\,T_{\gamma\gamma\to\pi\pi}\,]\;\cdot\;[\,T_{\pi\pi\to N\bar{N}}\,]^*\,. \tag{B9}$$

Combining the partial wave expansion for $\gamma\gamma \to \pi\pi$,

$$T^{\gamma\gamma\to\pi\pi}_{\Lambda_\gamma}(t,\theta_{\pi\pi}) \;=\; \sum_{Jeven}\,\frac{2J+1}{2}\,T^{J\,(\gamma\gamma\to\pi\pi)}_{\Lambda_\gamma}(t)\;\cdot\;\sqrt{\frac{(J-\Lambda_\gamma)!}{(J+\Lambda_\gamma)!}}\;\cdot\;P^{\Lambda_\gamma}_J(\cos\theta_{\pi\pi}), \tag{B10}$$

and the partial wave expansion for $\pi\pi \to N\bar{N}$,

$$T^{\pi\pi\to N\bar{N}}_{\Lambda_N}(t,\Theta) \;=\; \sum_{J}\,\frac{2J+1}{2}\,T^{J\,(\pi\pi\to N\bar{N})}_{\Lambda_N}(t)\;\cdot\;\sqrt{\frac{(J-\Lambda_N)!}{(J+\Lambda_N)!}}\;\cdot\;P^{\Lambda_N}_J(\cos\Theta)\,. \tag{B11}$$

We can now construct the imaginary parts of the Compton t-channel partial waves,

$$2\,\mathrm{Im}T^{J\,(\gamma\gamma\to N\bar{N})}_{\lambda_N\lambda_{\bar{N}},\,\lambda'_\gamma\lambda_\gamma}(t) \;=\; \frac{1}{(8\pi)}\,\frac{p_\pi}{\sqrt{t}}\left[\,T^{J\,(\gamma\gamma\to\pi\pi)}_{\Lambda_\gamma}(t)\,\right]\left[\,T^{J\,(\pi\pi\to N\bar{N})}_{\Lambda_N}(t)\,\right]^*. \tag{B12}$$

The partial wave amplitudes $T^{J\,(\pi\pi\to N\bar{N})}_{\Lambda_N}$ of Eq. (B11) are related to the amplitudes $f^J_\pm(t)$ of Frazer and Fulco [41] by the relations

$$\begin{aligned} T^{J\,(\pi\pi\to N\bar{N})}_{\Lambda_N=0}(t) &= \frac{16\pi}{p_N}\,(p_N\;p_\pi)^J\;\cdot\;f^J_+(t)\;,\\ T^{J\,(\pi\pi\to N\bar{N})}_{\Lambda_N=1}(t) &= 8\pi\,\frac{\sqrt{t}}{p_N}\,(p_N\;p_\pi)^J\;\cdot\;f^J_-(t)\;, \end{aligned} \tag{B13}$$

with p_N and p_π the c.m. momenta of nucleon and pion respectively,

$$p_N = \sqrt{t/4 - M^2}\,, \qquad\qquad p_\pi = \sqrt{t/4 - m_\pi^2}\,. \tag{B14}$$

For the reaction $\gamma\gamma \;\to\; \pi\pi$, we will use the partial wave amplitudes $F_{J\,\Lambda_\gamma}(t)$, which are related to those of Eq. (B10) by

$$T^{J\,(\gamma\gamma\to\pi\pi)}_{\Lambda_\gamma}(t) \;=\; \frac{2}{\sqrt{2J+1}}\cdot F_{J\,\Lambda_\gamma}(t)\,. \tag{B15}$$

Denoting the Born partial wave amplitudes for $\gamma\gamma \;\to\; \pi^+\pi^-$ by $B_{J\,\Lambda_\gamma}(t)$, the lowest Born partial waves (s and d waves) are

$$\begin{aligned} B_{00}(t) =&\; 2e^2\,\frac{1-\beta^2}{2\beta}\;\ln\left(\frac{1+\beta}{1-\beta}\right),\\ B_{20}(t) =&\; 2e^2\,\frac{\sqrt{5}}{4}\,\frac{1-\beta^2}{\beta^2}\;\left\{\,\frac{3-\beta^2}{\beta}\,\ln\left(\frac{1+\beta}{1-\beta}\right)\;-\;6\,\right\},\\ B_{22}(t) =&\; 2e^2\,\frac{\sqrt{15}}{4\sqrt{2}}\;\left\{\,\frac{(1-\beta^2)^2}{\beta^3}\,\ln\left(\frac{1+\beta}{1-\beta}\right)\;+\;\frac{10}{3}\;-\;\frac{2}{\beta^2}\,\right\}\,, \end{aligned} \tag{B16}$$

with $\beta = p_\pi / \left(\sqrt{t}/2\right)$ the pion velocity.

Inserting the partial-wave expansion of Eq. (B7) into Eq. (B6), we can finally express the 2π t-channel contributions $\mathrm{Im}_t A_i(\nu=0,t)^{2\pi}$ by the partial wave amplitudes for the reactions $\gamma\gamma \to \pi\pi$ and $\pi\pi \to N\bar{N}$,

$$\mathrm{Im}_t A_1(\nu=0,t)^{2\pi} = \frac{p_\pi}{\sqrt{t}} \frac{1}{t\, p_N^2} \sum_{J=0,2,4,\ldots} (p_\pi\, p_N)^J \sqrt{2J+1}\, F_{J\,\Lambda_\gamma=0}(t)\, f_+^{J*}(t) \left[(-1)^{J/2} \frac{(J-1)!!}{J!!}\right],$$

$$\mathrm{Im}_t A_2(\nu=0,t)^{2\pi} = 0\,,$$

$$\mathrm{Im}_t A_3(\nu=0,t)^{2\pi} =$$

$$\frac{p_\pi}{\sqrt{t}} \frac{M^2}{t\, p_N^4} \sum_{J=2,4,\ldots} (p_\pi\, p_N)^J \sqrt{2J+1}\;\; F_{J\,\Lambda_\gamma=2}(t) \left[(-1)^{(J-2)/2} \sqrt{\frac{(J+1)J}{(J-1)(J+2)}}\, \frac{(J-1)!!}{J!!}\right]$$
$$\times \left\{ f_+^{J*}(t) \;-\; f_-^{J*}(t)\; M \left[\frac{(J+2)(J-1)\;-\;2}{\sqrt{J(J+1)}}\right]\right\},$$

$$\mathrm{Im}_t A_4(\nu=0,t)^{2\pi} =$$

$$-\frac{p_\pi}{\sqrt{t}} \frac{M^3}{t\, p_N^4} \sum_{J=4,\ldots} (p_\pi\, p_N)^J \sqrt{2J+1}\, F_{J\,\Lambda_\gamma=2}(t)\, f_-^{J*}(t) \frac{(-1)^{(J-2)/2}\; 2\; (J-2)(J+3)}{\sqrt{(J+2)(J-1)}} \frac{(J-1)!!}{J!!},$$

$$\mathrm{Im}_t A_5(\nu=0,t)^{2\pi} =$$

$$-\frac{p_\pi}{\sqrt{t}} \frac{M}{t\, p_N^2} \sum_{J=2,4,\ldots} (p_\pi\, p_N)^J \sqrt{2J+1}\;\; F_{J\,\Lambda_\gamma=0}(t)\; f_-^{J*}(t) \left[\frac{(-1)^{(J-2)/2}}{\sqrt{J(J+1)}} \frac{(J+1)!!}{(J-2)!!}\right],$$

$$\mathrm{Im}_t A_6(\nu=0,t)^{2\pi} =$$

$$-\frac{p_\pi}{\sqrt{t}} \frac{M}{t\, p_N^2} \sum_{J=2,4,\ldots} (p_\pi\, p_N)^J \sqrt{2J+1}\;\; F_{J\,\Lambda_\gamma=2}(t)\; f_-^{J*}(t)$$
$$\times \left[\frac{(-1)^{(J-2)/2}\;\; [(J+2)(J-1)\;-\;2]}{\sqrt{(J+2)(J-1)}}\; \frac{(J-1)!!}{J!!}\right]. \qquad \text{(B17)}$$

We note that the s-wave ($J=0$) component of the 2π intermediate states contributes only to A_1. The amplitude A_2, corresponding to the exchange of pseudoscalar mesons (dominantly π^0) in the t-channel, gets no contribution from 2π states, because the 2π system cannot couple to the nucleon through a pseudoscalar operator. Furthermore, it is found that only waves with $J \geq 4$ contribute to the amplitude A_4. In our calculations we saturate the t-channel dispersion integral with s(J = 0)- and d($J=2$)-waves, for which the expressions of Eq. (B17) reduce to those given in Eq. (44).

APPENDIX C: F_2-MESON CONTRIBUTION TO THE $\gamma\gamma \to \pi\pi$ PROCESS

A particle with mass m and spin-2 is described in terms of a symmetric and traceless field tensor $\Phi^{\mu\nu}$ satisfying the Klein-Gordon equation. Furthermore, as for a massive spin-1 field, the 'Lorentz gauge' condition requires that the four-divergence with respect to one of the four-vector indices vanishes,

$$
\begin{aligned}
\left(\Box \, + \, m^2 \right) \, \Phi^{\mu\nu} \, &= \, 0 \, , \\
\Phi^{\mu\nu} \, &= \, \Phi^{\nu\mu} \, , \\
\Phi^{\mu}{}_{\mu} \, &= \, 0 \, , \\
\partial_\mu \, \Phi^{\mu\nu} \, &= \, \partial_\nu \, \Phi^{\mu\nu} \, = \, 0 \, .
\end{aligned}
\tag{C1}
$$

Therefore, the tensor $\Phi^{\mu\nu}$ has only five independent components.

A state of spin-2 is characterized by its polarization tensor $\varepsilon^{\mu\nu}\,(p,\Lambda)$, where $\Lambda \; = \; \{2,1,0,-1,-2\}$ defines the polarization,

$$
\begin{aligned}
\varepsilon^{\mu\nu}\,(p,\Lambda) \, &= \, \varepsilon^{\nu\mu}\,(p,\Lambda) \, , \\
\varepsilon^{\mu}{}_{\mu}\,(p,\Lambda) \, &= \, 0 \, , \\
p_\mu \, \varepsilon^{\mu\nu}\,(p,\Lambda) \, &= \, p_\nu \, \varepsilon^{\mu\nu}\,(p,\Lambda) \, = \, 0 \, .
\end{aligned}
\tag{C2}
$$

The polarization tensor $\varepsilon^{\mu\nu}\,(p,\Lambda)$ can be constructed from (massive) spin-1 polarization vectors by

$$
\varepsilon^{\mu\nu}\,(p,\Lambda) \; = \; \sum_{\lambda=-1,0,1} \; \sum_{\lambda'=-1,0,1} \; \langle \; 1\,\lambda, \; 1\,\lambda' \; | \; 2\,\Lambda \; \rangle \; \epsilon^{\mu}\,(p,\lambda) \; \epsilon^{\nu}\,(p,\lambda') \; . \tag{C3}
$$

If one chooses the z-axis along the momentum of the particle, the three polarization vectors of a massive spin-1 particle are

$$
\begin{aligned}
\epsilon^{\mu}\,(p,\lambda \, = \, +1) \; &= \; (\; 0 \, , \, -\frac{1}{\sqrt{2}} \, , \, -\frac{i}{\sqrt{2}} \, , \, 0 \;) \; , \\
\epsilon^{\mu}\,(p,\lambda \, = \, -1) \; &= \; (\; 0 \, , \, +\frac{1}{\sqrt{2}} \, , \, -\frac{i}{\sqrt{2}} \, , \, 0 \;) \; , \\
\epsilon^{\mu}\,(p,\lambda \, = \, 0) \; &= \; (\; |\vec{p}| , \; 0, \; 0, \; p^0 \;) \; / \; m \; ,
\end{aligned}
\tag{C4}
$$

where $p^\mu \, = \, (p^0, 0, 0, |\vec{p}|)$ and $p^2 \, = \, m^2$. In the case of the spin-2 polarization tensor constructed as in Eq. (C3), the following normalization and completeness conditions hold :

$$
\begin{aligned}
\varepsilon^{\mu\nu}\,(p,\Lambda) \; \cdot \; \varepsilon^{*}_{\mu\nu}\,(p,\Lambda') \; &= \; \delta_{\Lambda\Lambda'} \; , \\
\sum_{\Lambda} \, \varepsilon^{\mu\nu}\,(p,\Lambda) \, [\, \varepsilon^{\alpha\beta}\,(p,\Lambda) \,]^* \; &= \; \frac{1}{2} \, \left(\; K^{\mu\alpha} \, K^{\nu\beta} \; + \; K^{\nu\alpha} \, K^{\mu\beta} \; - \; \frac{2}{3} \, K^{\mu\nu} \, K^{\alpha\beta} \; \right) \; , \\
\text{with} \;\; K^{\mu\nu} \; &= \; - \, g^{\mu\nu} \; + \; \frac{p^\mu p^\nu}{m^2} \; .
\end{aligned}
\tag{C5}
$$

Finally, the propagator of the spin-2 particle with total width Γ takes the form

$$
i \; \Delta^{\mu\nu\alpha\beta}\,(p) \; = \; \frac{i \; \sum_\Lambda \, [\, \varepsilon^{\mu\nu}\,(p,\Lambda) \,]^* \; \varepsilon^{\alpha\beta}\,(p,\Lambda)}{p^2 \; - \; m^2 \; + \; i \, m \, \Gamma} \; . \tag{C6}
$$

We will now apply this spin-2 formalism to describe the s-channel exchange of the f_2 meson in the process $\gamma\gamma \, \to \, \pi\pi$.

The coupling of the (isoscalar) $f_2(1270)$ meson to a pion pair (with momenta p_π, p'_π and cartesian isospin indices a, b) is described by the amplitude

$$\mathcal{M}\,(f_2\,\rightarrow\,\pi\pi)\;=\;\frac{g_{f_2\pi\pi}}{m_{f_2}}\,\delta_{ab}\,{p'_\pi}^{\,\mu}\,p_\pi^\nu\,\varepsilon_{\mu\nu}\,(p,\Lambda)\;, \tag{C7}$$

where p is the f_2 meson momentum and m_{f_2} its mass. The coupling constant $g_{f_2\pi\pi}$ is determined from the $f_2\,\rightarrow\,\pi\pi$ decay width :

$$\Gamma(f_2\,\rightarrow\,\pi\pi)\;=\;\frac{1}{40\pi}\,g^2_{f_2\pi\pi}\,\frac{(p_\pi)^5}{m^4_{f_2}}\;, \tag{C8}$$

where $p_\pi\,=\,\sqrt{m^2_{f_2}/4-m^2_\pi}$ is the pion momentum in the f_2 rest frame. Using the partial width $\Gamma(f_2\,\rightarrow\,\pi\pi)\;=\;0.846\,\Gamma_0$ and the total f_2-width $\Gamma_0\;=\;185$ MeV [25], Eq. (C8) yields for the coupling : $g_{f_2\pi\pi}\simeq 23.64$.

The Lorentz structure of the vertex $f_2\,\rightarrow\,\gamma\gamma$ is given by

$$\mathcal{M}\,(f_2\,\rightarrow\,\gamma\gamma)\;=\;-i\,2\,e^2\,\frac{g_{f_2\gamma\gamma}}{m_{f_2}}\,\mathcal{F}^{\mu\delta}\,(q,\lambda_\gamma)\,\mathcal{F}_\delta{}^\nu\,\left(q',\lambda'_\gamma\right)\;\varepsilon_{\mu\nu}\,(p,\Lambda)\;, \tag{C9}$$

where $\mathcal{F}^{\alpha\beta}$ is the electromagnetic field tensor :

$$\mathcal{F}^{\alpha\beta}\,(q,\lambda_\gamma)\;=\;q^\alpha\,\varepsilon^{\beta *}\,(q,\lambda_\gamma)\;-\;q^\beta\,\varepsilon^{\alpha *}\,(q,\lambda_\gamma)\;. \tag{C10}$$

Using the vertex of Eq. (C9), the $f_2\,\rightarrow\,\gamma\gamma$ decay width is calculated as :

$$\Gamma(f_2\,\rightarrow\,\gamma\gamma)\;=\;\frac{e^4}{80\pi}\,g^2_{f_2\gamma\gamma}\,m_{f_2}. \tag{C11}$$

Using the partial width $\Gamma(f_2\,\rightarrow\,\gamma\gamma)\;=\;1.32\cdot 10^{-5}\;\Gamma_0$ [25], Eq. (C11) determines the value of the coupling constant : $g_{f_2\gamma\gamma}\simeq 0.239$.

Using these couplings and vertices, we can now calculate the invariant amplitude for the process $\gamma\gamma\,\rightarrow\,f_2\,\rightarrow\,\pi\pi$:

$$\mathcal{M}\,(\gamma\gamma\xrightarrow{f_2}\pi\pi)\;=\;-i\,2\,e^2\,\frac{g_{f_2\gamma\gamma}}{m_{f_2}}\,\mathcal{F}^{\mu\delta}(q,\lambda_\gamma)\mathcal{F}_\delta{}^\nu(q',\lambda'_\gamma)\;\Delta_{\mu\nu\alpha\beta}(p,\Lambda)\;\frac{g_{f_2\pi\pi}}{m_{f_2}}\,p^\alpha_\pi\,{p'_\pi}^{\,\beta}\,. \tag{C12}$$

To determine the $\gamma\gamma\,\rightarrow\,\pi\pi$ helicity amplitudes F_{Λ_γ} defined in Eq. (32), we shall evaluate Eq. (C12) in the c.m. system. For the case of equal photon helicities ($\Lambda_\gamma\,=\,0$) the f_2 does not contribute, i.e.

$$F^{(f_2)}_{\Lambda_\gamma\,=\,0}\;=\;0\;. \tag{C13}$$

For the case of opposite photon helicities ($\Lambda_\gamma\,=\,2$) we find after some algebra :

$$F^{(f_2)}_{\Lambda_\gamma\,=\,2}\;=\;-\frac{e^2}{8}\,\frac{g_{f_2\gamma\gamma}\,g_{f_2\pi\pi}}{m^2_{f_2}}\,\frac{t^2\beta^2}{t\,-\,m^2_{f_2}\,+\,im_{f_2}\Gamma_0}\,\sin^2\theta_{\pi\pi}\;, \tag{C14}$$

where $\theta_{\pi\pi}$ is the pion c.m. angle and β the pion velocity as in Eq. (32). It is immediately seen from Eq. (C14) that the f_2 meson contribution to the d-wave is given by :

$$F^{(f_2)}_{J=2\;\Lambda_\gamma=2}(t)\;=\;-\sqrt{\frac{2}{15}}\,\frac{e^2}{4}\,\frac{g_{f_2\gamma\gamma}\,g_{f_2\pi\pi}}{m^2_{f_2}}\,\frac{t^2\beta^2}{t\,-\,m^2_{f_2}\,+\,im_{f_2}\Gamma_0}\;. \tag{C15}$$

REFERENCES

[1] F.J. Federspiel et al., Phys. Rev. Lett. **67**, 1511 (1991).
[2] A. Zieger et al., Phys. Lett. B **278**, 34 (1992).
[3] E.L. Hallin et al., Phys. Rev. C **48**, 1497 (1993).
[4] B.E. MacGibbon et al., Phys. Rev. C **52**, 2097 (1995).
[5] A. L'vov, V.A. Petrun'kin and M. Schumacher, Phys. Rev. C **55**, 359 (1997).
[6] C. Molinari et al., Phys. Lett. B **371**, 181 (1996).
[7] J. Peise et al., Phys. Lett. B **384**, 37 (1996).
[8] J. Tonnison, A.M. Sandorfi, S. Hoblit and A.M. Nathan, Phys. Rev. Lett. **80**, 4382 (1998).
[9] V.Bernard, N. Kaiser and U.-G. Meissner, Phys. Rev. Lett. **67**, 1515 (1991).
[10] V.Bernard, N. Kaiser, J. Kambor and U.-G. Meissner, Nucl. Phys. B **388**, 315 (1992).
[11] V.Bernard, N. Kaiser, A. Schmidt, U.-G. Meissner, Phys. Lett. B **319**, 269 (1993); Z. Phys. A **348**, 317 (1994).
[12] T.R. Hemmert, B.R. Holstein and J. Kambor, Phys. Lett. B **395**, 89 (1997).
[13] T.R. Hemmert, B.R. Holstein and J. Kambor, Phys. Rev. D **55**, 5598 (1997).
[14] T.R. Hemmert, B.R. Holstein, J. Kambor and G. Knöchlein, Phys. Rev. D **57**, 5746 (1998).
[15] V.Bernard, N. Kaiser, J. Kambor and U.-G. Meissner, Int. J. Mod. Phys. E **4**, 193 (1995).
[16] D. Drechsel, G. Krein and O. Hanstein, Phys. Lett. B **420**, 248 (1998).
[17] A.I. L'vov and A.M. Nathan, Phys. Rev. C **59**, 1064 (1999).
[18] A.M. Baldin, Nucl. Phys. **18**, 310 (1960); L.I. Lapidus, Sov. Phys. JETP **16**, 964 (1963).
[19] M. Damashek and F.J. Gilman, Phys. Rev. D **1**, 1319 (1970).
[20] D. Babusci, G. Giordano and G. Matone, Phys. Rev. C **57**, 291 (1998).
[21] A.M. Sandorfi, C.S. Whisnant and M. Khandaker, Phys. Rev. D **50**, R6681 (1994).
[22] J. Ahrens et al., MAMI proposal 12/2-93 (1993); H.J. Arends, Proceedings of the 8th International Conference on the Structure of Baryons (Baryons 98), Bonn, Germany, 22-26 Sep. 1998.
[23] D. Babusci, G. Giordano, A.I. L'vov, G. Matone and A.M. Nathan, Phys. Rev. C **58**, 1013 (1998).
[24] B.R. Holstein and A.M. Nathan, Phys. Rev. D **49**, 6101 (1994).
[25] Particle Data Group, C. Caso et al., Eur. Phys. J. C **3**, 1 (1998).
[26] R.A. Arndt, R.L. Workman, I.I. Strakovsky, M.M. Pavan, nucl-th/9807087.
[27] S. Ragusa, Phys. Rev. D **47**, 3757 (1993); Phys. Rev. D **49**, 3157 (1994).
[28] O. Hanstein, D. Drechsel, L. Tiator, Nucl. Phys. A **632**, 561 (1998).
[29] R.A. Arndt, I.I. Strakovsky and R.L. Workman, Phys. Rev. C **53**, 430 (1996).
[30] D. Drechsel, S.S. Kamalov, G. Krein, L. Tiator, hep-ph/9810480.
[31] R.A. Arndt, R.L. Workman, Z. Li, and L.D. Roper, Phys. Rev. C **42**, 1853 (1990); Phys. Rev. C **42**, 1864 (1990).
[32] D. Drechsel, G. Krein, Phys. Rev. D **58**, 11609 (1998).
[33] D. Morgan and M.R. Pennington, Z. Phys. C **37**, 431 (1988).
[34] M.R. Pennington, in *The Second Da*Φ*ne Physics Handbook*, Eds. L. Maiani, G. Pancheri, N. Paver (INFN, Frascati, 1995).
[35] C.D. Froggatt and J.L. Petersen, Nucl. Phys. B **129**, 89 (1977).

[36] G. Höhler, *Pion-Nucleon Scattering*, Landolt-Börnstein, Vol.I/9b2, ed. H. Schopper, Springer (1983).
[37] V. Olmos de Léon, private communication.
[38] G. Blanpied et al., Phys. Rev. Lett. **79**, 4337 (1997); Phys. Rev. Lett. **76**, 1023 (1996).
[39] J. Ahrens, private communication.
[40] R.E. Prange, Phys. Rev. **110**, 240 (1958).
[41] W.R. Frazer and J.R. Fulco, Phys. Rev. **117**, 1603 (1960).

TABLES

TABLE I. The contribution of the dispersion integrals to the spin polarizabilities of the proton. The set HDT(1π) is calculated from the one-pion photoproduction multipoles of the HDT analysis [28], while the column HDT gives the total results with the additional contribution of inelastic resonance channels. The entries in the last column are the predictions of the dispersion calculation of Ref. [23].

γ_i – excit.	HDT(1π)	HDT	Ref. [23]
$\gamma_1^{(p)}$	+4.83	+4.33	+3.1
$\gamma_2^{(p)}$	-0.81	-0.74	-0.8
$\gamma_3^{(p)}$	-0.30	-0.02	+0.3
$\gamma_4^{(p)}$	+3.19	+2.93	+2.7
$\gamma_o^{(p)}$	-0.75	-0.80	-1.5
$\gamma_{13}^{(p)}$	+4.23	+4.29	+3.7
$\gamma_{14}^{(p)}$	-1.56	-1.53	-2.3
$\gamma_\pi^{(p)}$	+10.41	+9.46	+7.8

TABLE II. The same as in Table I in the case of the neutron.

γ_i – excit.	HDT(1π)	HDT	Ref. [23]
$\gamma_1^{(n)}$	+7.10	+7.00	+6.3
$\gamma_2^{(n)}$	-0.68	-0.68	-0.9
$\gamma_3^{(n)}$	-1.04	-0.99	-0.7
$\gamma_4^{(n)}$	+3.92	+3.88	+3.8
$\gamma_o^{(n)}$	-0.06	-0.09	-0.4
$\gamma_{13}^{(n)}$	+5.02	+5.02	+4.9
$\gamma_{14}^{(n)}$	-0.74	-0.77	-1.3
$\gamma_\pi^{(n)}$	+14.27	+14.09	+13.0

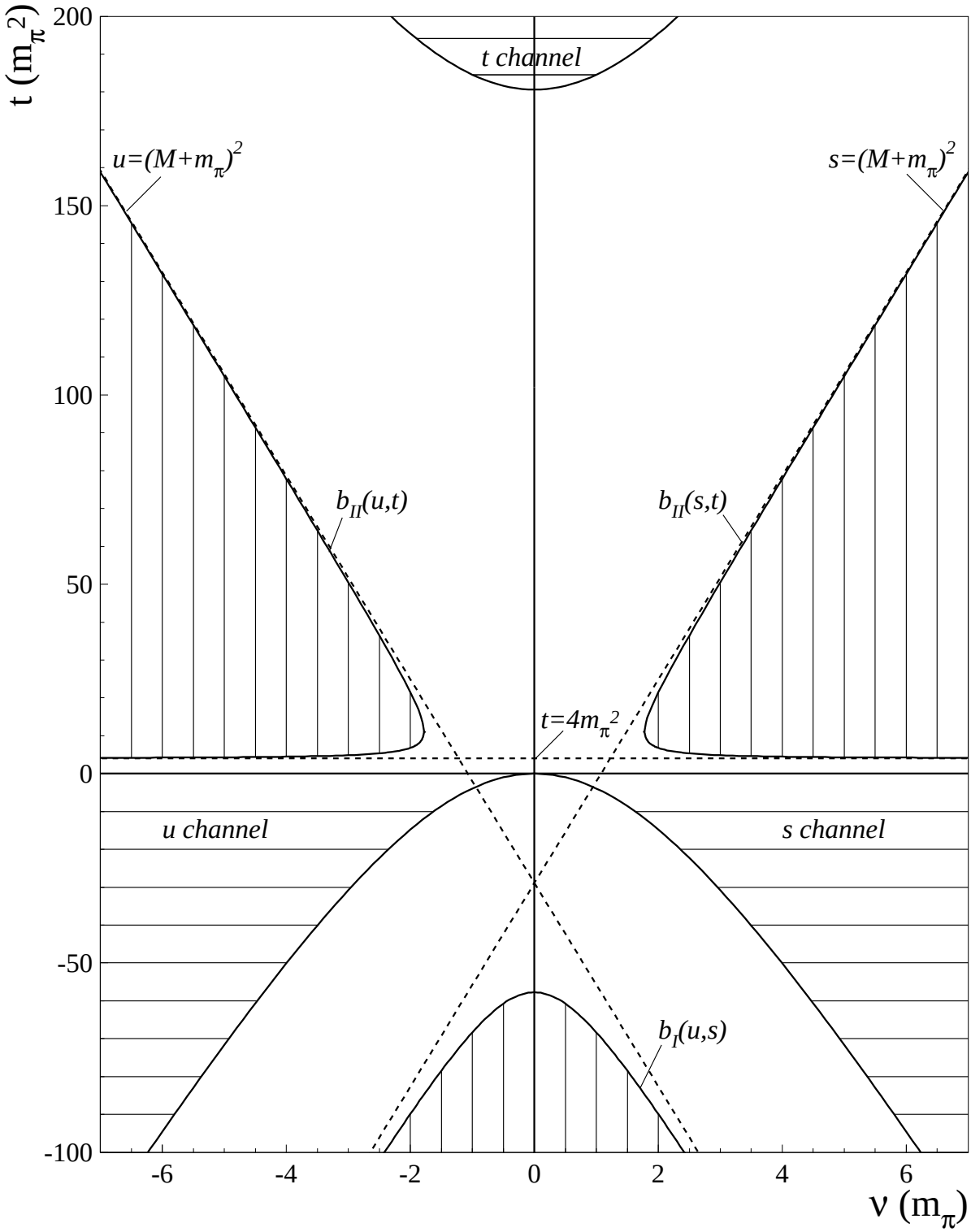

FIG. 1. The Mandelstam plane for Compton scattering. The physical regions are horizontally hatched, whereas the spectral regions are vertically hatched.

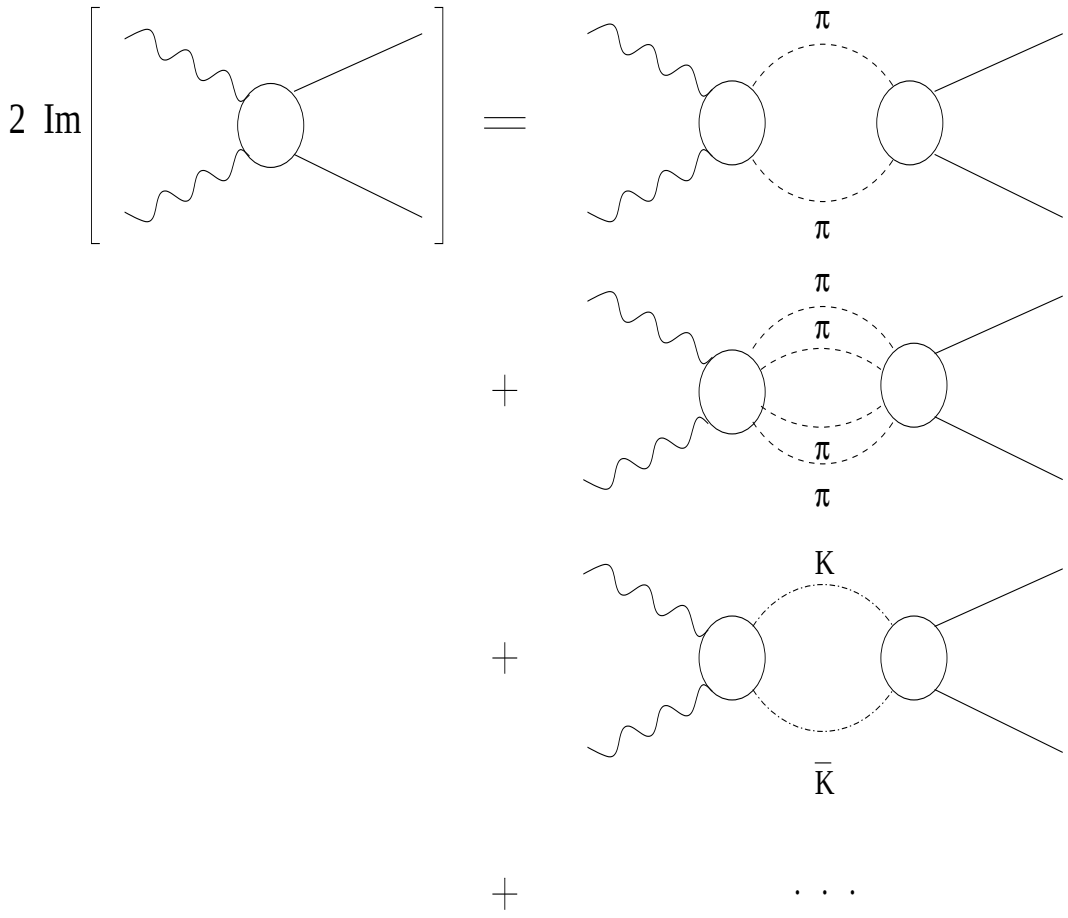

FIG. 2. t-channel unitarity diagrams for Compton scattering.

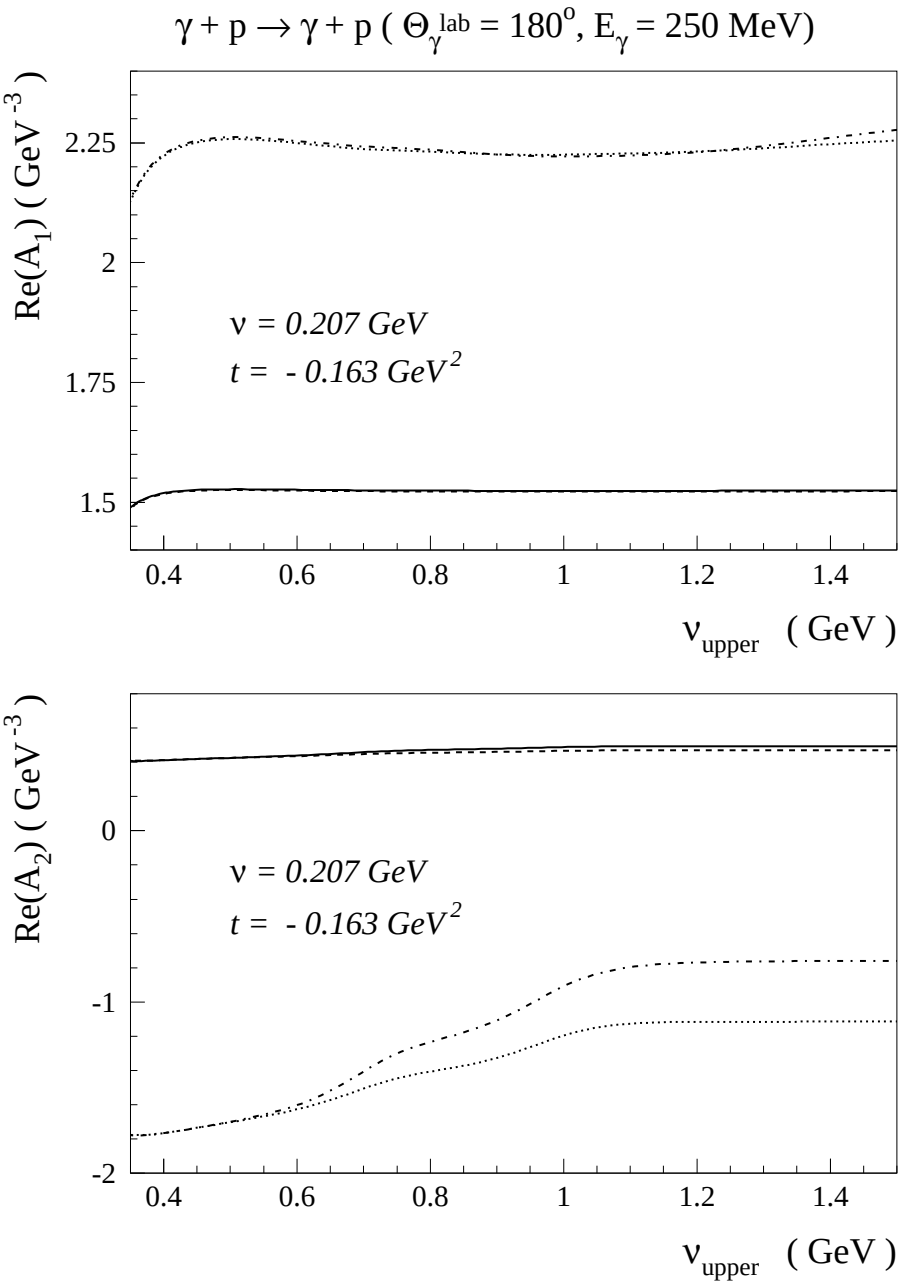

FIG. 3. Convergence of the s-channel integral for the amplitudes A_1 and A_2. Results for the unsubtracted dispersion integral of Eq. (10) for the one-pion channel (dotted lines) and including the two-pion channel (dashed-dotted lines) in comparison with the subtracted dispersion integral of Eq. (15) for the one-pion channel (dashed line) and including the two-pion channel (full lines), as function of the upper integration limit $\nu_{\rm upper}$.

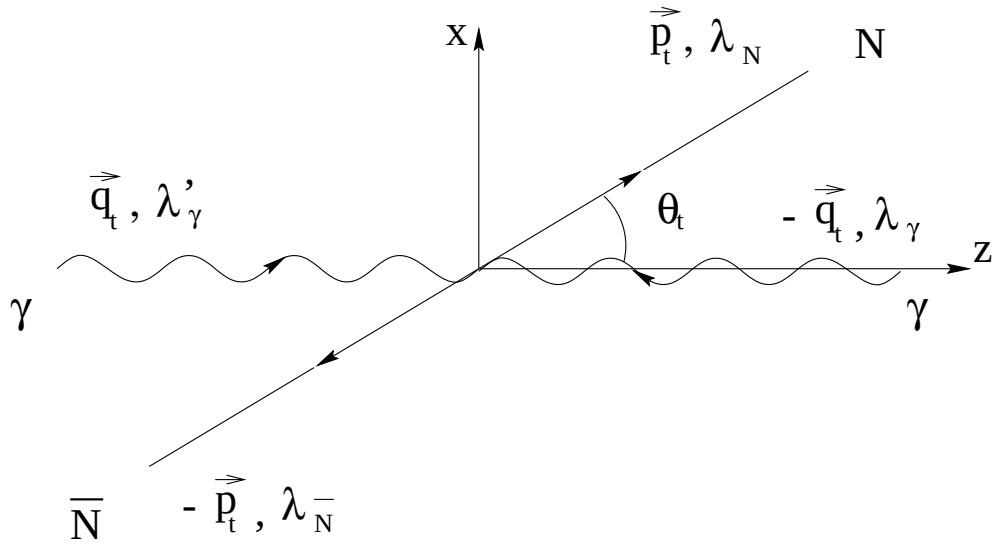

FIG. 4. Kinematics in the c.m. system of the t-channel process $\gamma\gamma \to N\bar{N}$.

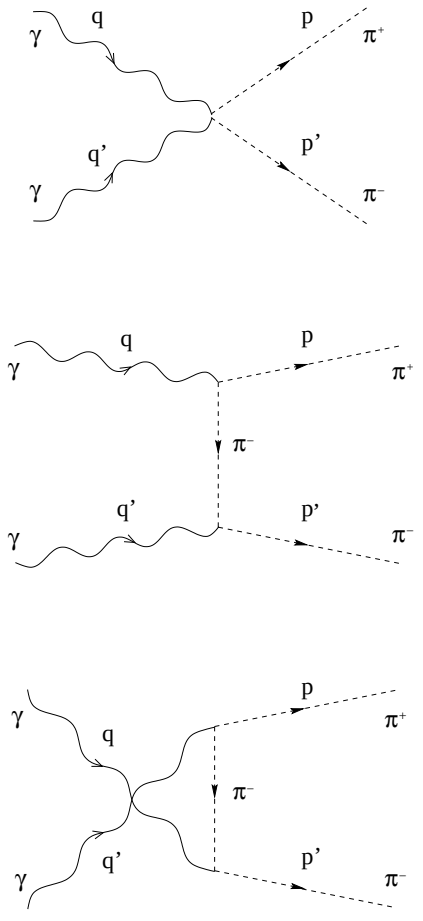

FIG. 5. Born diagrams for the $\gamma\gamma \to \pi^+\pi^-$ process.

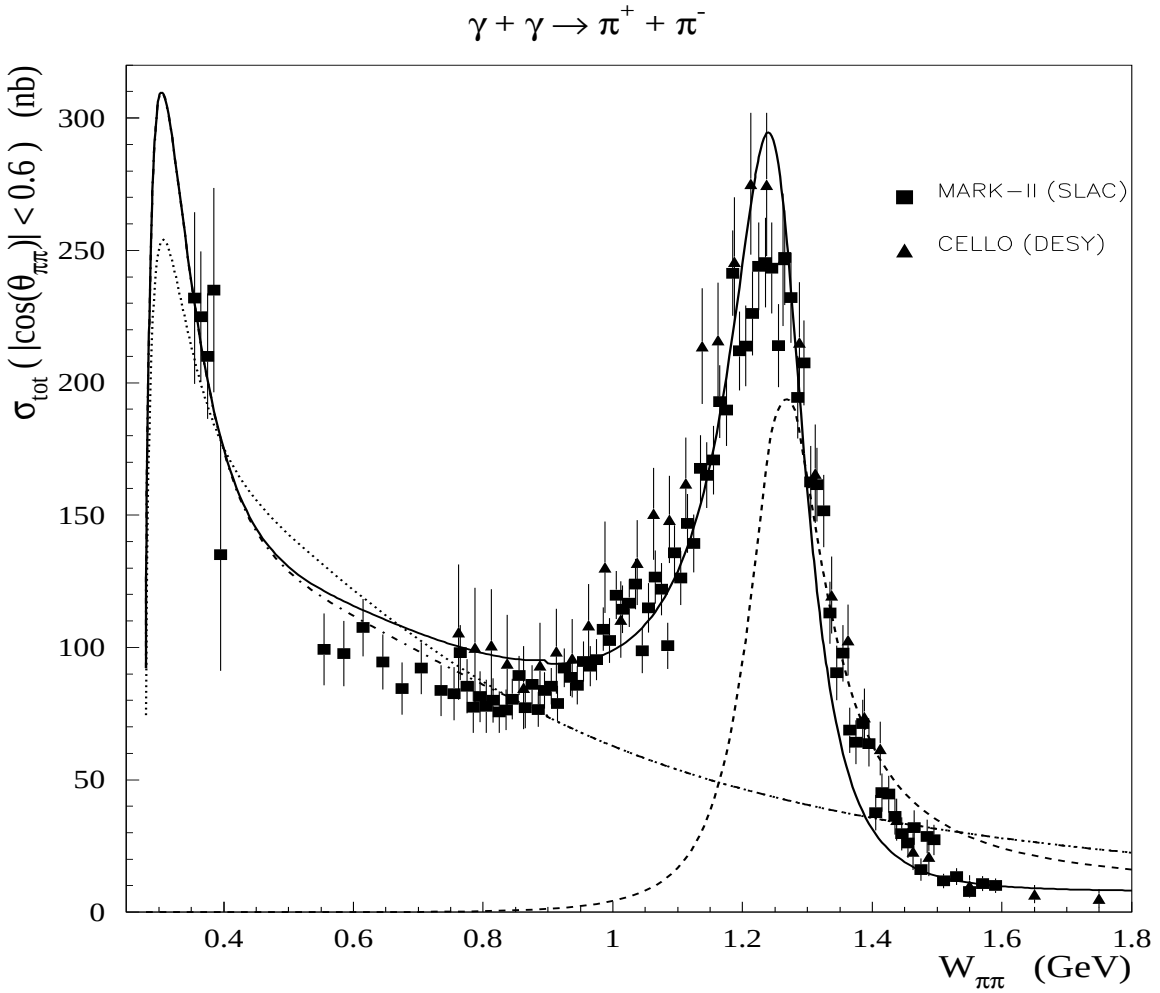

FIG. 6. Total cross section for the $\gamma\gamma \to \pi^+\pi^-$ process as function of the c.m. energy : Born terms (dotted line), Born amplitude with unitarized s-wave (dashed-dotted line), $f_2(1270)$ resonance contribution (dashed line) and total amplitude (full line).

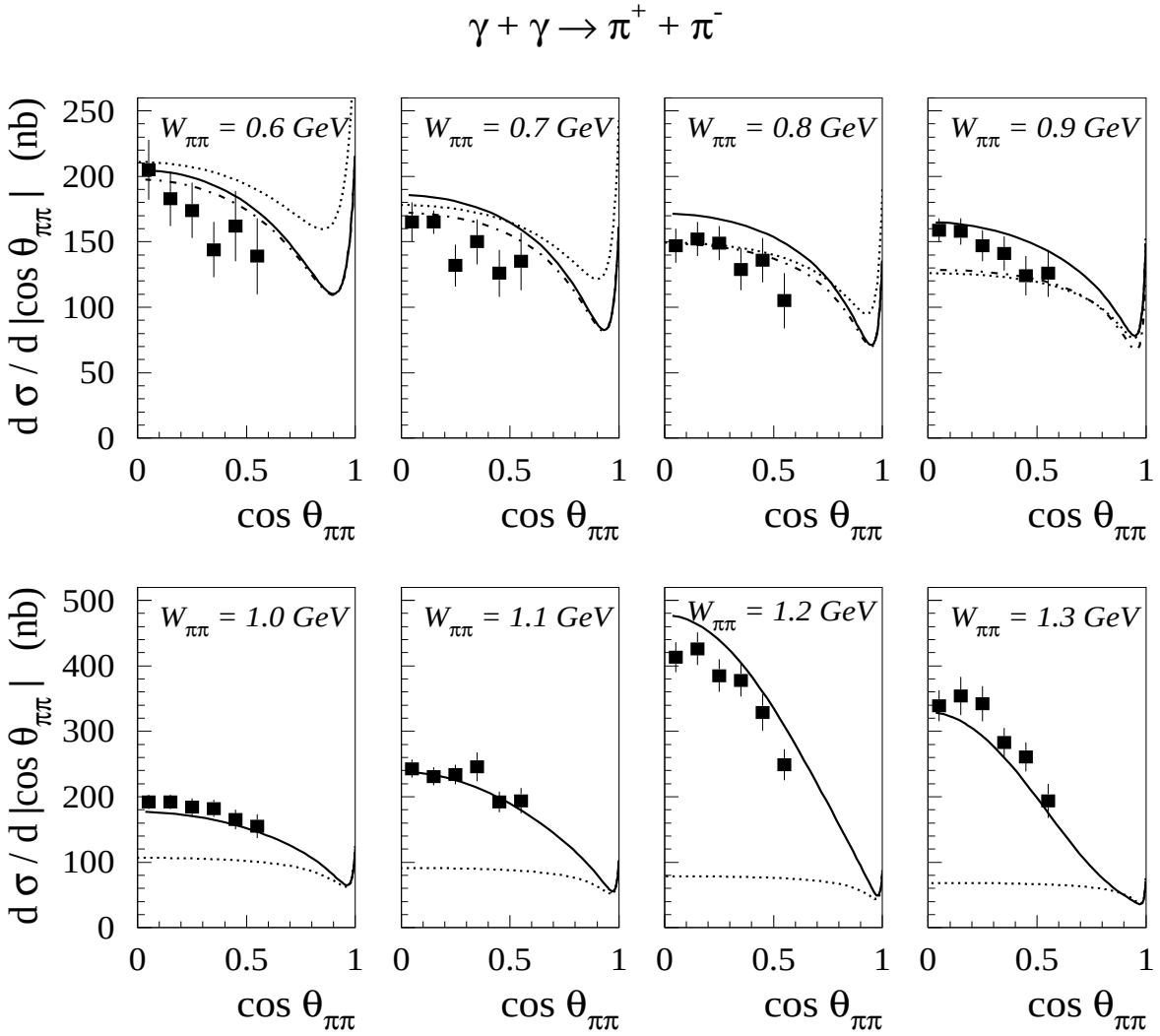

FIG. 7. Differential cross section at various c.m. energies for the $\gamma\gamma \to \pi^+\pi^-$ process : Born terms (dotted line), Born amplitude with unitarized s-wave (dashed-dotted line, only shown at the four lower energies), and total amplitude including the $f_2(1270)$ resonance contribution (full line).

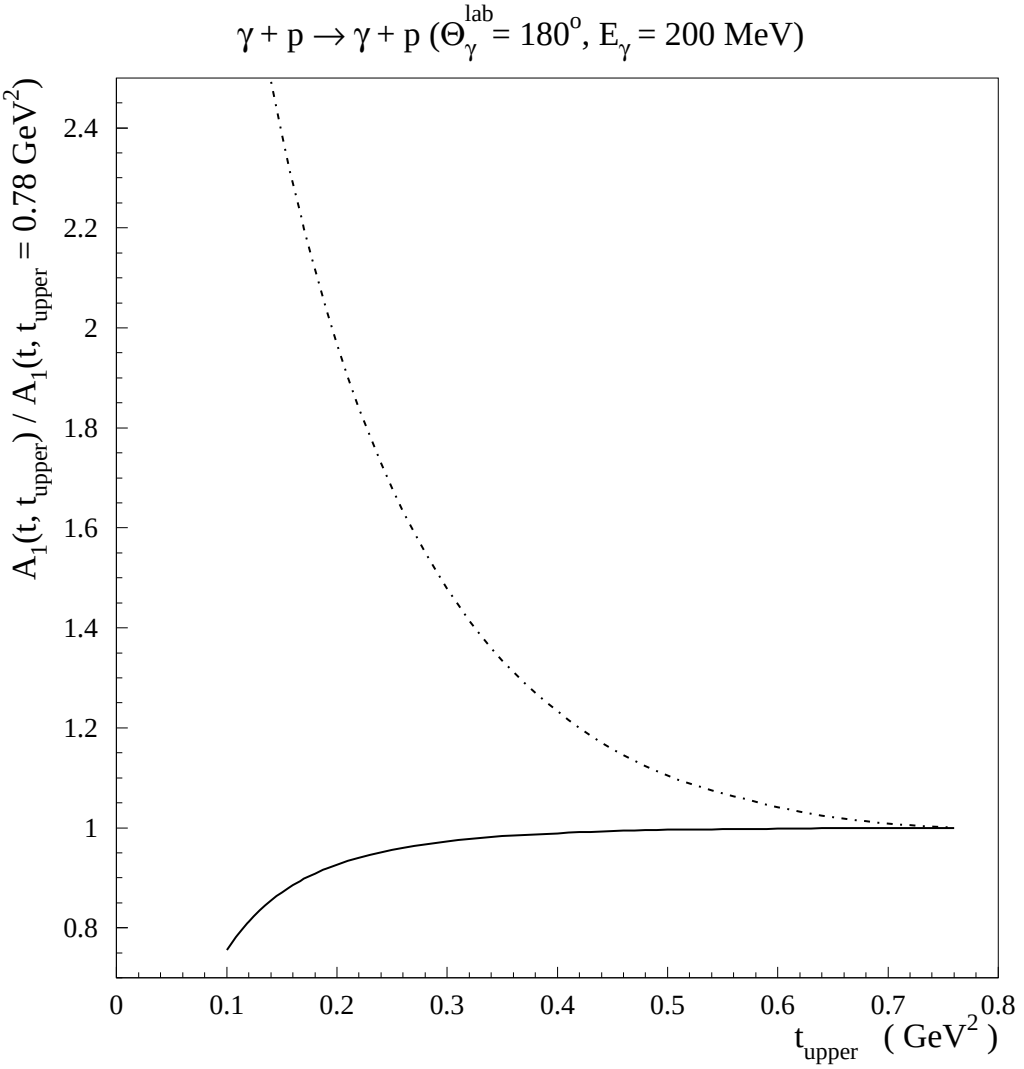

FIG. 8. Convergence of the t-channel integral for the amplitude A_1. Results for the unsubtracted (dashed curve) and the subtracted (full curve) t-channel dispersion integrals are shown as function of the upper integration limit $t_{\rm upper}$. Both results are normalized to their respective values at $t_{\rm upper} = 0.78$ GeV^2.

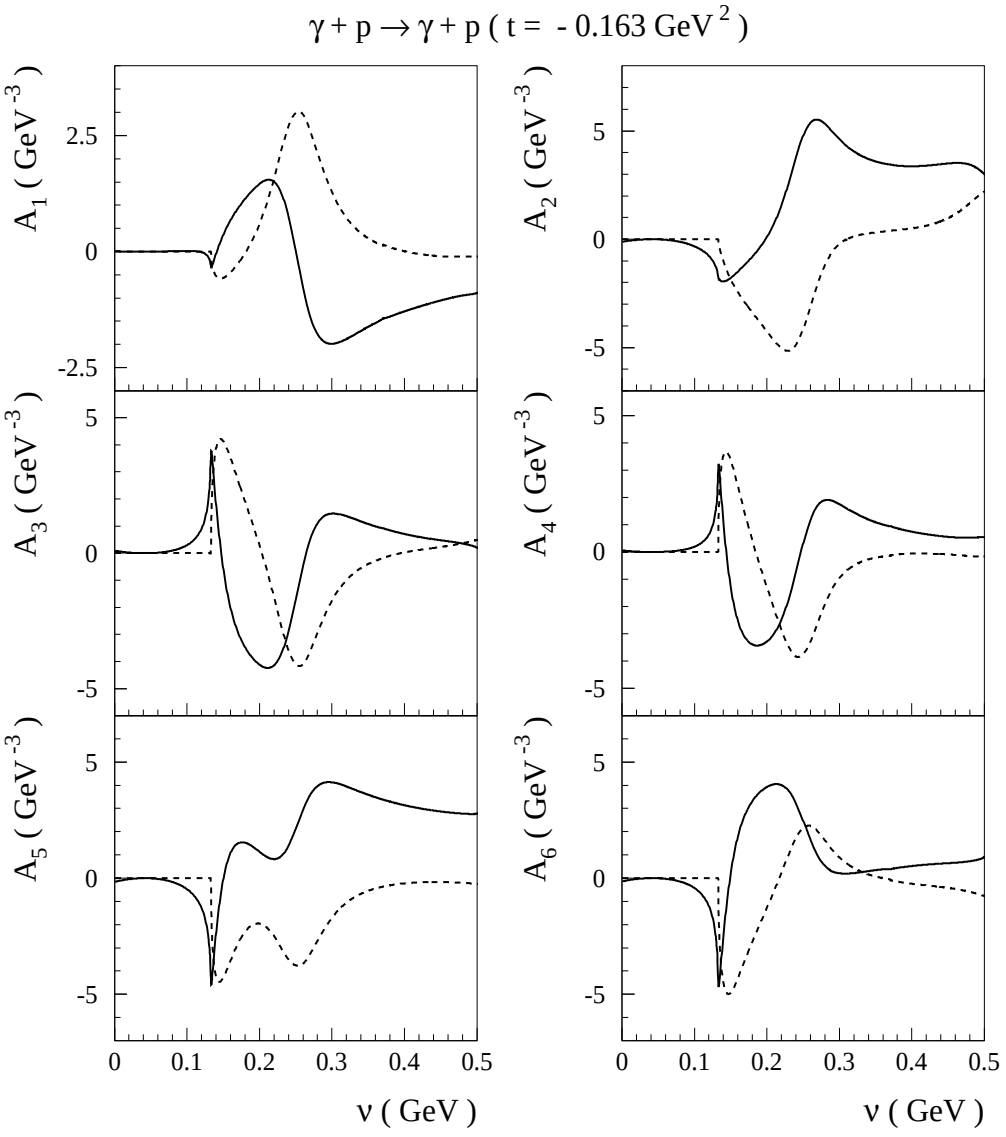

FIG. 9. Real parts (full lines) of the subtracted s-channel integral of Eq. (15) and imaginary parts (according to Eq. (28)) to the invariant Compton amplitudes $A_1, ..., A_6$ as function of ν at fixed t = -0.163 GeV^2.

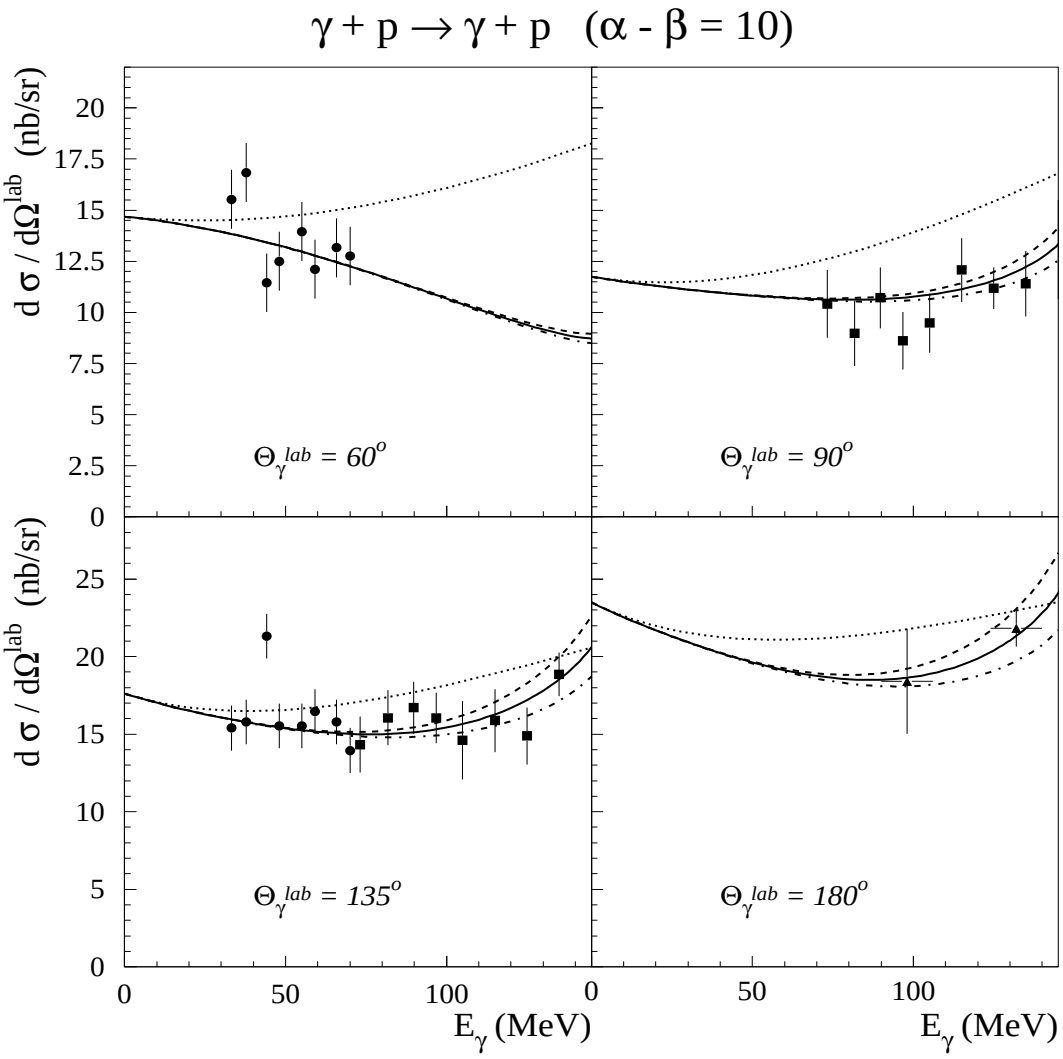

FIG. 10. Differential cross section for Compton scattering off the proton as function of the lab photon energy E_γ and at 4 scattering angles Θ_γ^{lab}. The Born result is given by the dotted lines. The total results of the subtracted dispersion formalism are shown for fixed $\alpha - \beta = 10$ and different values of γ_π : γ_π = -37 (dashed-dotted lines), γ_π = -32 (full lines) and γ_π = -27 (dashed lines). The data are from Ref. [1] (circles), Ref. [2] (triangles) and Ref. [4] (squares).

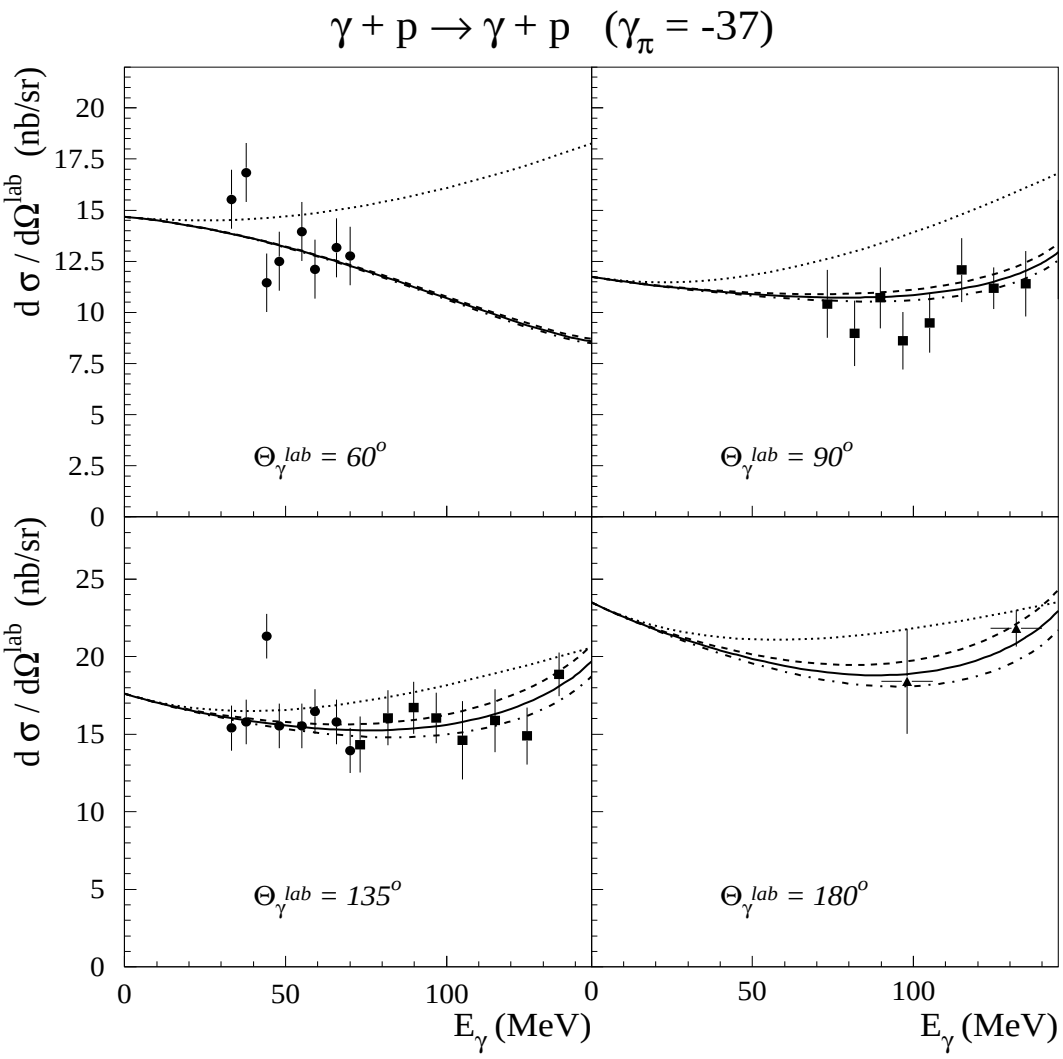

FIG. 11. Differential cross section for Compton scattering off the proton as function of the lab photon energy E_γ and at 4 scattering angles Θ_γ^{lab} as in Fig. 10. The Born result is given by the dotted lines. The total results of the subtracted dispersion formalism are presented for fixed $\gamma_\pi = -37$ and different values of $\alpha - \beta$: $\alpha - \beta = 10$ (dashed-dotted lines), $\alpha - \beta = 8$ (full lines), and $\alpha - \beta = 6$ (dashed lines). Data as described in Fig. 10.

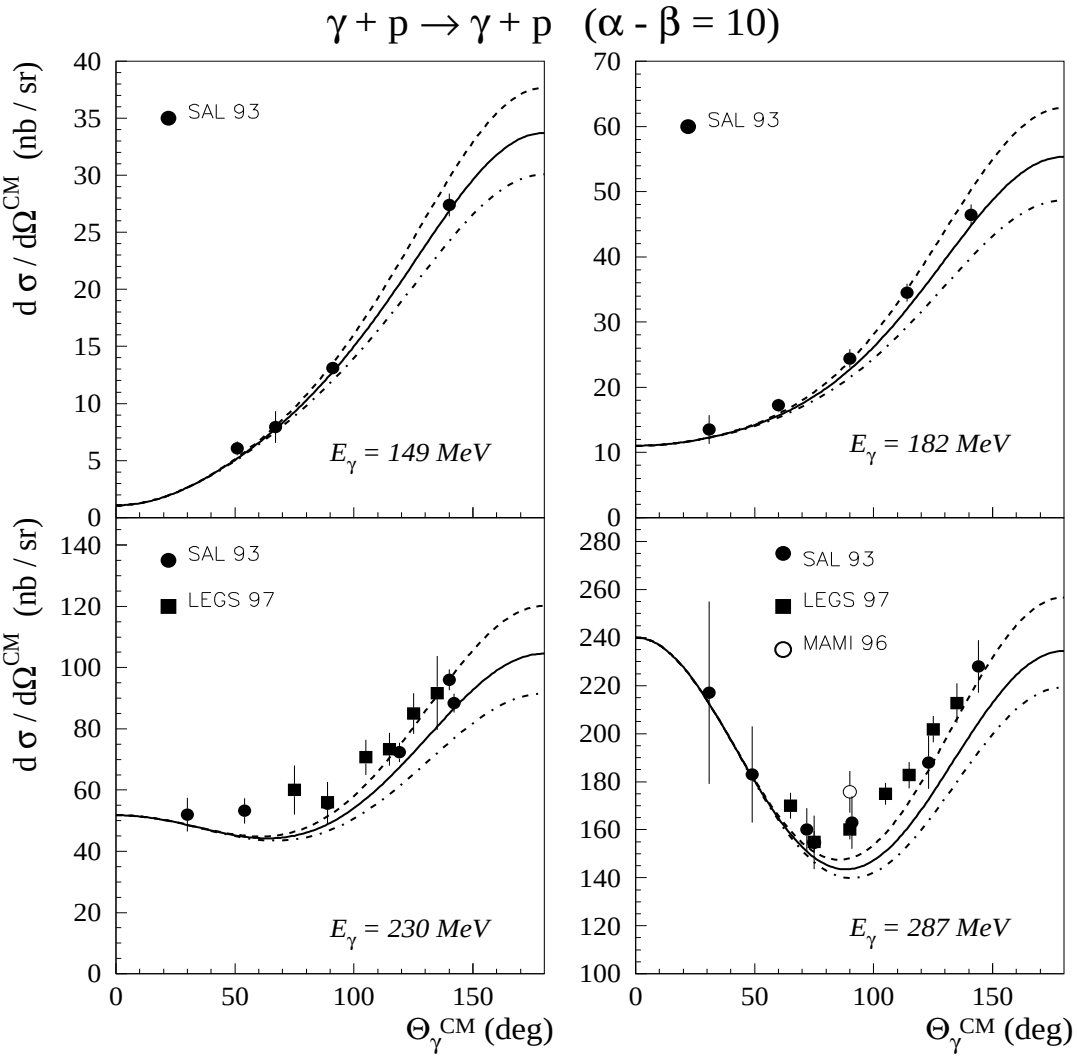

FIG. 12. Differential cross section for Compton scattering off the proton as function of the c.m. photon angle for different lab energies. The total results of the subtracted DR formalism are presented for fixed $\alpha - \beta = 10$ and different values of γ_π : γ_π = -37 (dashed-dotted lines), γ_π = -32 (full lines) and γ_π = -27 (dashed lines). The data are from Ref. [3] (solid circles), Refs. [6,7] (open circles) and Ref. [8] (squares).

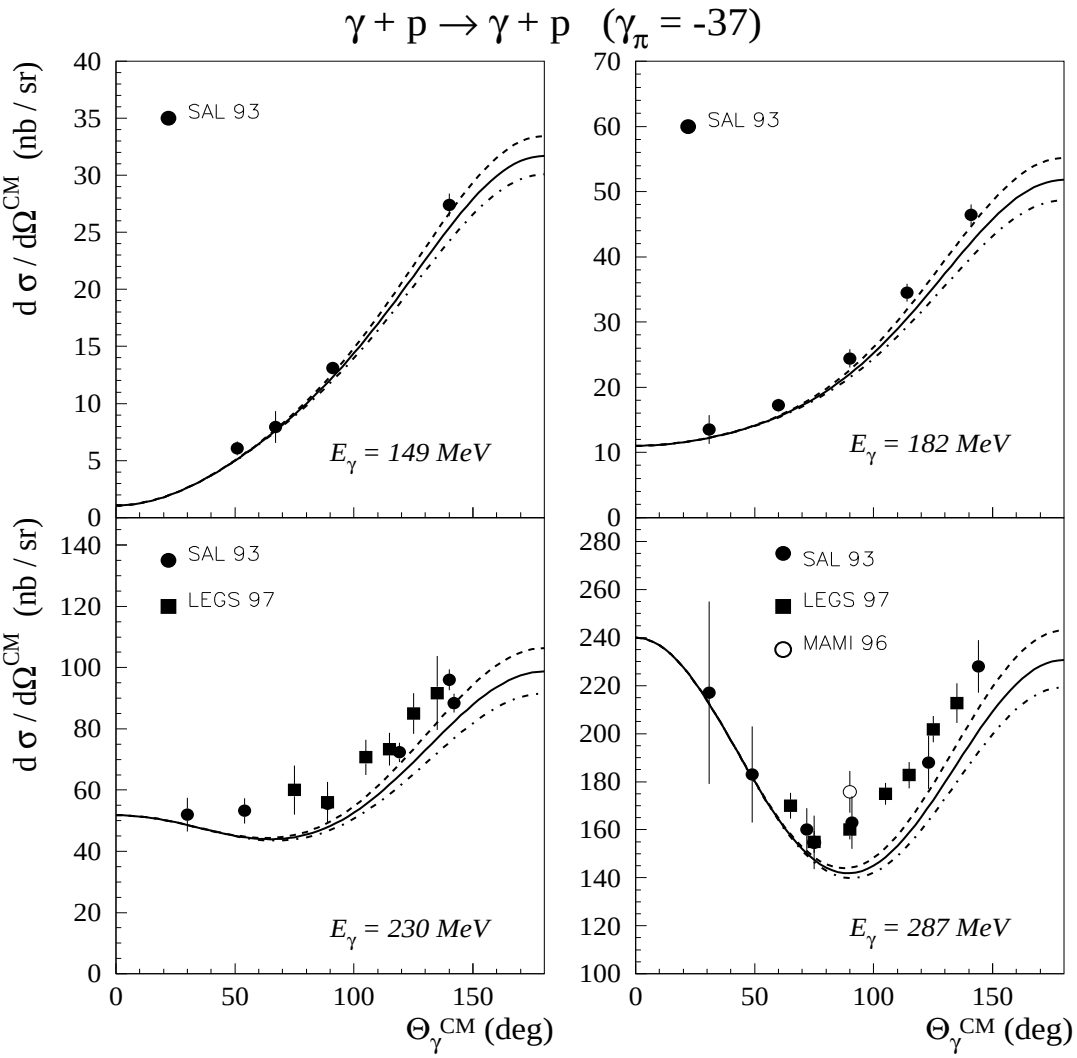

FIG. 13. Differential cross section for Compton scattering off the proton as function of the c.m. photon angle for different lab energies as in Fig. 12. The total results of the subtracted DR formalism are presented for fixed $\gamma_\pi = -37$ and different values of $\alpha-\beta$: $\alpha-\beta = 10$ (dashed-dotted lines), $\alpha - \beta = 8$ (full lines), and $\alpha - \beta = 6$ (dashed lines). Data as described in Fig. 12.

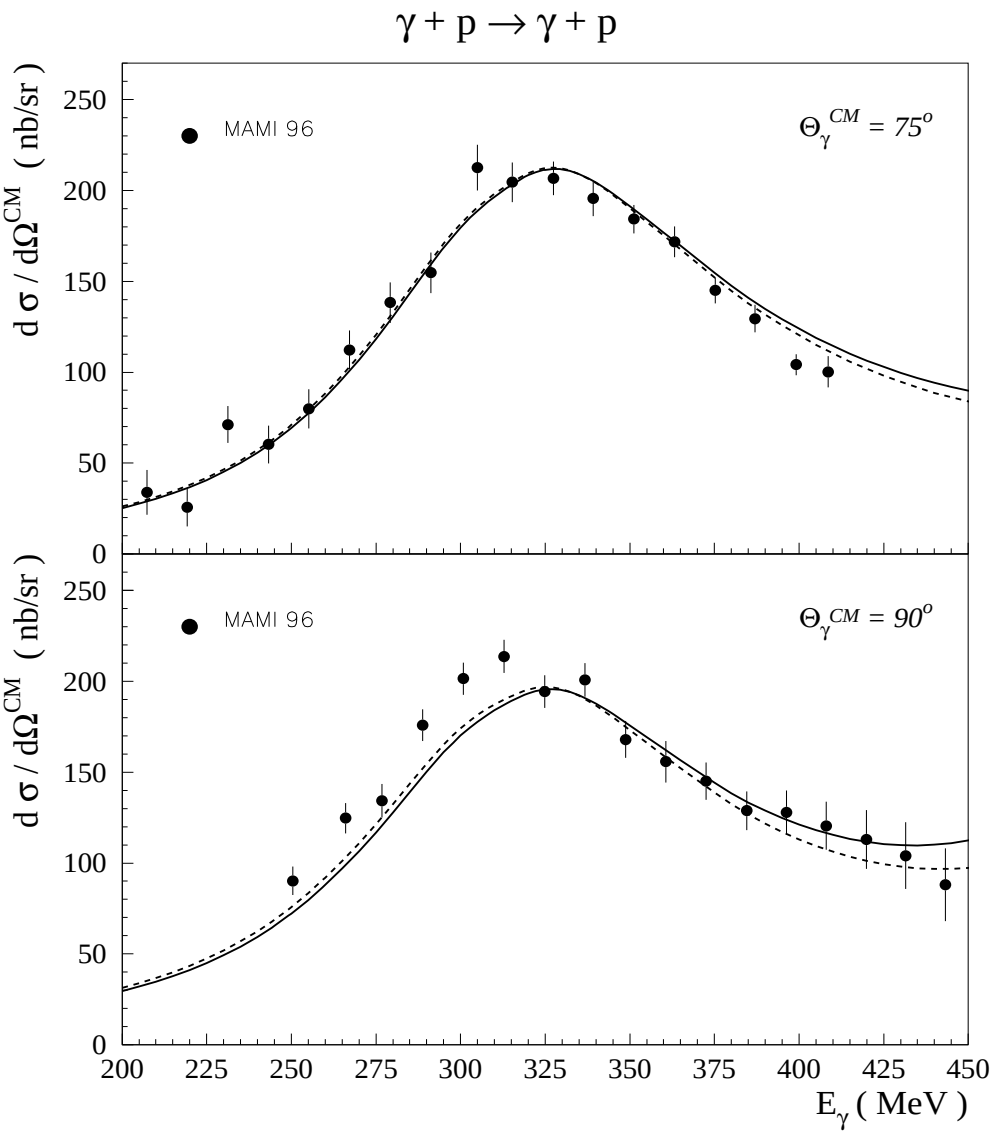

FIG. 14. Differential cross sections for Compton scattering off the proton at fixed c.m. scattering angle through the Δ resonance region. The total results of the subtracted DR formalism are shown for fixed $\alpha - \beta = 10$ and different values of γ_π : γ_π = -32 (full lines) and γ_π = -27 (dashed lines). The MAMI data are from [7] (upper panel) and [6] (lower panel).

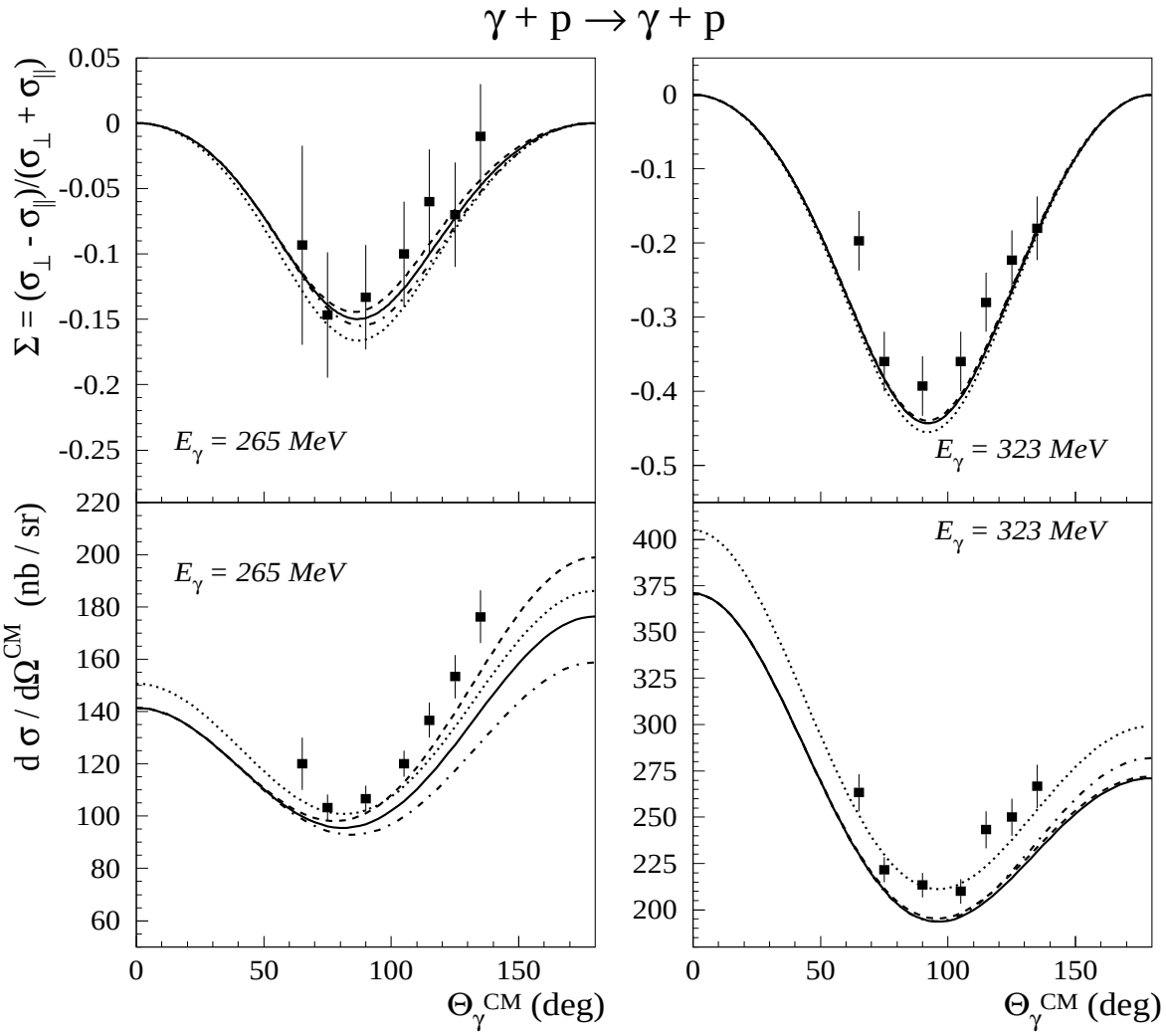

FIG. 15. Photon asymmetries (upper panels) and differential cross sections (lower panels) for Compton scattering off the proton in the Δ resonance region. The total results of the subtracted DR formalism are shown for fixed $\alpha - \beta = 10$ and different values of γ_π : γ_π = -37 (dashed-dotted lines), γ_π = -32 (full lines) and γ_π = -27 (dashed lines). We also show the result for $\alpha - \beta = 10$ and γ_π = -32 when increasing the HDT M_{1+} multipole by 2.5 % (dotted lines). The data are from LEGS 97 [38].

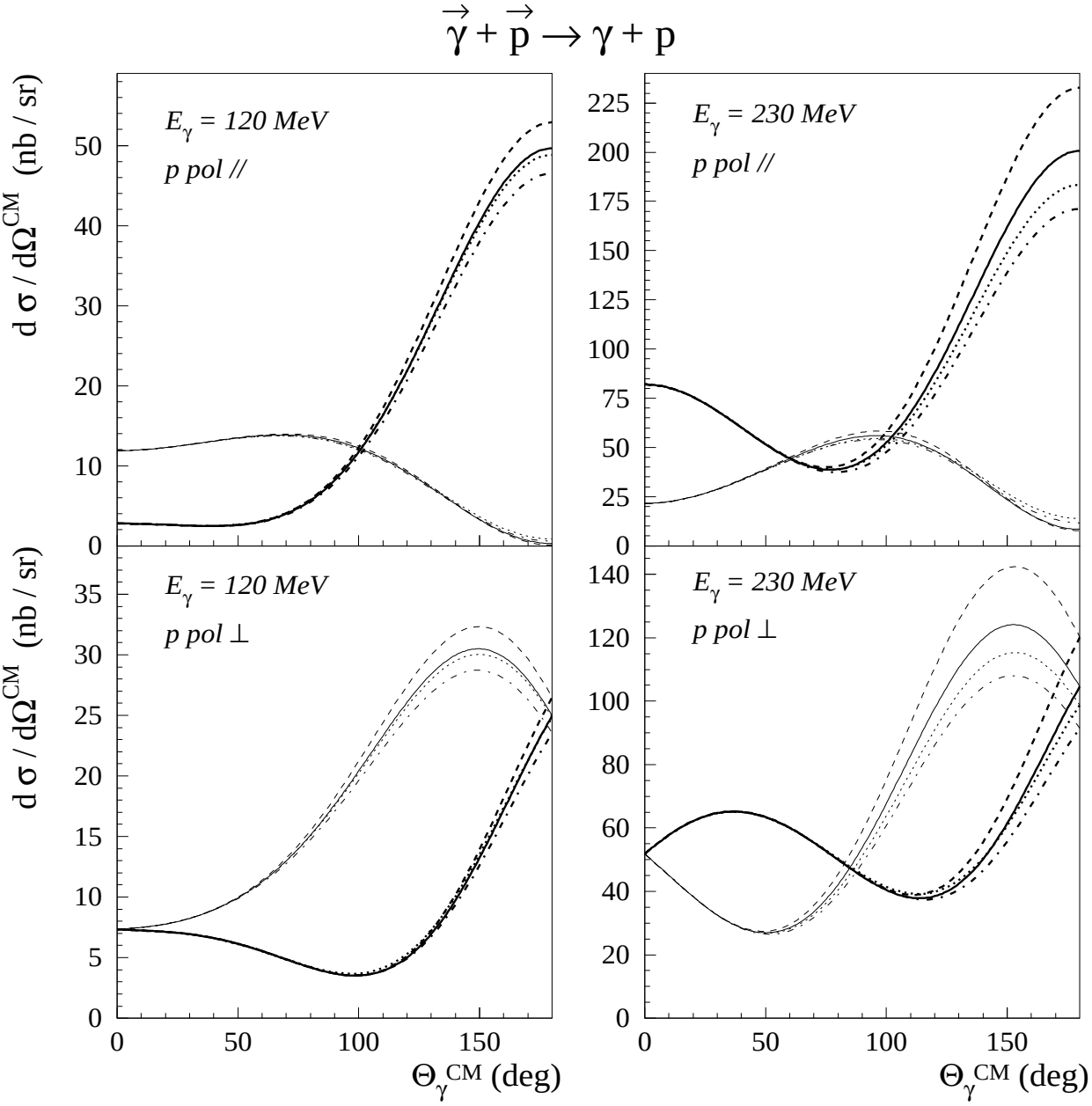

FIG. 16. Double polarization differential cross sections for Compton scattering off the proton, with circularly polarized photon and target proton polarized along the the photon direction (upper panels) or perpendicular to the photon direction and in the plane (lower panels). The thick (thin) lines correspond to a proton polarization along the positive (negative) direction respectively. The results of the dispersion calculation are for $\alpha - \beta = 10$ and different values for γ_π : γ_π = -32 (full lines), γ_π = -27 (dashed lines) and γ_π = -37 (dashed-dotted lines). We also show the result for $\alpha - \beta = 8$ and γ_π = -37 (dotted lines).